AGU PUBLICATIONS

Journal of Advances in Modeling Earth Systems

RESEARCH ARTICLE
10.1002/2016MS000839

This article is a companion to *Wong et al.* [2017], doi:10.1002/2016MS000842.

Key Points:
- Water isotope physics has been added to version 5 of the Community Atmosphere Model
- Water isotopes can differentiate the causes of a model's hydrologic biases
- Water isotopes are sensitive to atmospheric convection and moisture transport

Correspondence to:
J. Nusbaumer,
jesse.nusbaumer@nasa.gov

Citation:
Nusbaumer, J., T. E. Wong, C. Bardeen, and D. Noone (2017), Evaluating hydrological processes in the Community Atmosphere Model Version 5 (CAM5) using stable isotope ratios of water, *J. Adv. Model. Earth Syst.*, *9*, 949–977, doi:10.1002/2016MS000839.

Received 20 OCT 2016
Accepted 14 MAR 2017
Accepted article online 3 APR 2017
Published online 28 APR 2017
Corrected 10 APR 2019

This article was corrected on 10 APR 2019. See the end of the full text for details.

Evaluating hydrological processes in the Community Atmosphere Model Version 5 (CAM5) using stable isotope ratios of water

Jesse Nusbaumer[1,2], Tony E. Wong[3,4], Charles Bardeen[5], and David Noone[1,6]

[1]Department of Atmospheric and Oceanic Sciences and Cooperative Institute for Research in Environmental Sciences, Boulder, Colorado, USA, [2]Now at: NASA Goddard Institute for Space Studies, New York, New York, USA, [3]Now at: Earth and Environmental Systems Institute, Pennsylvania State University, University Park, Pennsylvania, USA, [4]Department of Applied Mathematics and Cooperative Institute for Research in Environmental Sciences, Boulder, Colorado, USA, [5]Atmospheric Chemistry Observations & Modeling Laboratory, National Center for Atmospheric Research, Boulder, Colorado, USA., [6]Now at: College of Earth, Ocean, and Atmospheric Sciences, Oregon State University, Corvallis, Oregon, USA

Abstract Water isotope-enabled climate and earth system models are able to directly simulate paleoclimate proxy records to aid in climate reconstruction. A less used major advantage is that water isotopologues provide an independent constraint on many atmospheric and hydrologic processes, allowing the model to be developed and tuned in a more physically accurate way. This paper describes the new isotope-enabled CAM5 model, including its isotopic physics routines, and its ability to simulate the modern distribution of water isotopologues in vapor and precipitation. It is found that the model has a negative isotopic bias in precipitation. This bias is partially attributed to model overestimates of deep convection, particularly over the midlatitude oceans during winter. This was determined by examining isotope ratios both in precipitation and vapor, instead of precipitation alone. This enhanced convective activity depletes the isotopic water vapor in the lower troposphere, where the majority of poleward moisture transport occurs, resulting in the insufficient transport of water isotopologue mass poleward and landward. This analysis also demonstrates that large-scale dynamical or moisture source changes can impact isotopologue values as much as local shifts in temperature or precipitation amount. The diagnosis of limitations in the large-scale transport characteristics has major implications if one is using isotope-enabled climate models to examine paleoclimate proxy records, as well as the modern global hydroclimate.

1. Introduction

Isotopes of hydrogen and oxygen in water have been found to provide unique information on the environmental conditions experienced by a given mass of water. Since the 1950s, researchers have examined the potential benefits of measuring and observing water isotopologues (water molecules that contain an isotope of hydrogen or oxygen) and water isotope ratios (the ratio of heavy isotope amount over the more abundant light isotope amount) to better understand the oceans [*Craig and Gordon*, 1965], precipitation [*Dansgaard*, 1964], land-surface water masses, such as rivers [*International Atomic Energy Agency* (*IAEA*), 2012], and the fluxes between all the major reservoirs in the earth system [e.g., *Merlivat and Jouzel*, 1979]. One of the major strengths of water isotopologues is that their signal can be recorded over a long period of time in certain environmental systems, allowing for the use of water isotope ratios as a paleoclimate record. These water isotopes ratio-based proxy records can be found in ice cores, ocean, and lake sediment cores, speleothems, corals, and tree cellulose [e.g., *Dee et al.*, 2015]. Thus, improving our knowledge of water isotope ratios and leveraging that knowledge can help increase our understanding of the earth system, both in the past and the present. This enhanced understanding can then be used to improve our predictions of the future.

Water isotope ratios are sensitive to many physical processes. This includes the history of phase changes experienced by the water mass of interest, the type of phase changes that occur, and the temperature and relative humidity during the phase changes. This problem can be confounded even more by the fact

that processes such as atmospheric or oceanic circulations can result in moisture source and sink changes, which can be difficult to disentangle if one only has a single point measurement, or an overly simplistic model. These processes also influence the distribution of water vapor and moist convection in the atmosphere, so by better understanding how they influence water isotope ratios one could also better understand climate changes and feedbacks, such as the water vapor feedback [*Sherwood et al*., 2010].

One way to account for the interplay between the many processes affecting the atmospheric water cycle is to use the additional information provided by the stable isotope chemistry of water, and to make use of an isotope-enabled Global Climate Model (GCM) or earth system model, which has the capability to simulate all the relevant physical processes, including the impact of circulation changes. The development and use of isotope-enabled GCMs has been progressing since the 1980s [*Joussame*, 1984], and now many different GCMs can simulate water isotopologues, at least in the atmosphere [e.g., *Noone and Sturm*, 2010; *Risi et al*., 2012a; *Conroy et al*., 2013]. Much of the focus of these models has been to try and understand paleoclimate proxy records, including possible uncertainties in their use as paleothermometers or hydrologic indicators [e.g., *Sime et al*., 2009].

GCMs have substantial errors, however, particularly when it comes to simulating unresolved, or subgrid scale, processes. Many of these processes have a direct influence on water isotope ratios, specifically cloud physical and convective processes [e.g., *Bolot et al*., 2013]. Thus, one can use water isotope ratios to help constrain model processes and diagnose model errors or biases. This approach has been illustrated succinctly in studies using several different GCMs. For example, *Risi et al*. [2012b], used a wide set of different isotopic observations along with the isotope-enabled LMDZ4 model to determine that the vertical diffusion in the model was too high. Similarly, *Field et al*. [2014], showed a high sensitivity for water isotope ratios in vapor to multiple different physics parameters in the isotope-enabled GISS model. These types of studies show much promise, and understanding these processes is vital, particularly when using the models to project future climate conditions. This is due to the potentially strong role convection and clouds have on climate feedbacks and sensitivity [*Sherwood et al*., 2010, 2014].

The opportunities for exploiting the advantages of isotope-enabled GCMs have been greatly increased given new isotopic observational platforms. Specifically, two new technologies have greatly expanded the spatial and temporal coverage of water isotope ratio measurements over the past decade. The first is the development of satellite instruments and retrieval algorithms that can deduce deuterium to hydrogen isotope ratios in atmospheric water vapor at scientifically relevant precision, allowing for near global coverage [*Worden et al*., 2006; *Frankenberg et al*., 2009; *Randel et al*., 2012]. The other development has been of in situ spectrometers that can provide isotopic vapor measurement in a continuous fashion [e.g., *Bailey et al*., 2015a], allowing for very detailed time series data at key locations around the globe, including deployments on mobile platforms [e.g., *Bailey et al*., 2013; *Kurita et al*., 2011]. These data create additional observational constraint on water isotope ratios in the atmosphere, allowing for new isotope-enabled model experiments that can more closely examine cloud and transport processes, using the additional information provided by the observed isotopic ratios.

This paper examines the simulation of atmospheric water isotopologues by the newly developed isotope-enabled Community Atmosphere Model, Version 5 (iCAM5), which is the atmospheric component of the isotope-enabled version of the National Center for Atmospheric Research's Community Earth System Model Version 1 (iCESM1). First, a description of the physics of water isotopologues and their implementation in iCAM5 is presented in section 2. Next, a comparison between an iCAM5 simulation of the modern climate and a suite of observations, including isotopic spectrometer and satellite data, is presented in section 3. This demonstrates the model's ability to simulate water isotope ratios correctly, but also quantifies the errors and biases present in the model itself. Then, in section 4, results from a parameter sensitivity analysis are described, with the key objective being to determine which model parameters have values that can be changed to minimize the mismatch between simulated water isotope ratios and observations. The sensitivity analysis demonstrates which processes water isotope ratios are most sensitive to in the model, and which processes iCAM5 may not be simulating properly. Finally, conclusions and a perspective on opportunities for further refinement and applications of models like iCAM5 are presented in section 5.

2. Isotopic Fractionation Physics in CAM

The Community Atmosphere Model Version 5 (CAM5) [*Neale et al*., 2010] is the atmospheric component of the NCAR Community Earth System Model (CESM) [*Hurrell et al*., 2013]. The broad strategy for implementing water isotopic tracers follows previous modeling work [e.g., *Joussaume et al*., 1984; *Jouzel et al*., 1987, 1991; *Hoffman et al*., 1998; *Noone and Simmonds*, 2002; *Yoshimura et al*., 2008; *Bony et al*., 2008] and in the description which follows, we give the manner in which fractionation has been added to the advanced parameterization schemes in CAM5. Water isotopologues, specifically HDO and $H_2^{18}O$, have been added and are tracked in all aspects of the model's hydrological cycle, including surface fluxes, condensation processes, and atmospheric transport. The standard water state variable in CAM5 is specific humidity (with a similar quantity for liquid and ice condensate). For isotope tracers, the state variable is similarly defined as specific humidity multiplied by the (molar) isotope ratio and normalized by a typical natural abundance (here assumed to be that of Vienna Standard Mean Ocean Water). Normalization by a standard ratio is algebraically arbitrary, but has the advantage of preserving precision within the various numerical schemes in CAM5. Transport by boundary layer turbulence and large-scale advection occurs without fractionation, and thus the water isotopologues are treated as conservative tracers.

Fractionation processes differentiate the abundance of heavy isotopologues from the more common species. Both equilibrium and kinetic fractionation are included, although the present version of the model omits mass-independent fractionation effects, which are considered to have limited influence on water in the troposphere [*Winkler et al*., 2013]. Equilibrium fractionation is theoretically very well understood [*Bigeleisen*, 1961] and is temperature dependent. The equilibrium fractionation factor, α_e, is the ratio of the saturation vapor pressure of the heavy isotopologue to normal water and in CAM5, we use values from empirical fits from the laboratory determinations of *Horita and Wesolowski* [1994] for liquid/vapor equilibration of $H_2^{18}O/H_2^{16}O$ and $HD^{16}O/H_2^{16}O$, *Majoube* [1971] for ice/vapor equilibration of $H_2^{18}O/H_2^{16}O$, and *Merlivat and Nief* [1967] for ice/vapor equilibration of $HD^{16}O/H_2^{16}O$.

Kinetic fractionation emerges from the fact that the diffusivity for water molecules with heavy isotopes is lower than the more abundant $H_2^{16}O$ water which leads to an isotopic separation when diffusion limits mobility. This results in a fractionation that occurs whenever the phase change occurring is not in thermodynamic equilibrium (i.e., relative humidity is not equal to 100%). In isotope-enabled CESM, kinetic fractionation occurs during oceanic evaporation, evaporation and transpiration from land, the deposition of vapor onto ice, and during the evaporation of rain into a subsaturated environment. The details of these fractionations are described below.

2.1. Surface Evaporation and Condensation

Ocean evaporation is calculated using the bulk aerodynamic formula [*Neale et al*., 2010]:

$$E = \rho_a C_E \Delta q \tag{1}$$

where ρ_a is the atmospheric surface density, C_E is the exchange coefficient, and Δq is the difference between the specific humidity at the lowest model layer, and the specific humidity in a thin surface layer that is at 98% relative humidity with respect to the ocean surface. The same formulation is used for water isotopologues, except that the equation for water isotopologues follows the *Craig and Gordon* [1965] hypothesis that the near surface vapor is in isotopic equilibrium with sea water, and is written as:

$$\Delta q_i = q_i - \frac{R_{ocn}}{\alpha_e} q_s \tag{2}$$

$$E_i = \alpha_k \rho_a C_e \Delta q_i \tag{3}$$

where q_i is the bottom atmospheric layer isotopic specific humidity, R_{ocn} is the isotopic ratio for the ocean surface, α_e is the equilibrium fractionation factor at the ocean surface temperature, q_s is the bulk water saturated layer humidity, and α_k is a kinetic fractionation factor. Kinetic fractionation is parametrized following *Merlivat and Jouzel* [1979], and is calculated as:

$$\alpha_k = 1 - \frac{\left(\left(\frac{D}{D_i}\right)^n - 1\right)}{\left(\frac{D}{D_i}\right)^n + M} \tag{4}$$

$$M = \frac{\frac{1}{k}\ln\left(\frac{u_* z_b}{30\nu}\right)}{13.6Sc^{2/3}} \quad If \;\; Re < 1 \tag{5}$$

$$M = \frac{\frac{1}{k}\ln\left(\frac{z_b}{z_0} - 5\right)}{7.3Re^{1/4}Sc^{1/2}} \quad If \;\; Re \geq 1 \tag{6}$$

$$z_0 = \frac{u_*^2}{81.1g} \tag{7}$$

$$\nu = \frac{1.7 * 10^{-5}}{\rho_a} \tag{8}$$

$$Re = \frac{u_* z_0}{\mu} \tag{9}$$

$$Sc = \frac{\mu}{D} \tag{10}$$

where D is the molecular diffusivity of regular water in air and D_i is the molecular diffusivity of isotopic water [*Merlivat*, 1978], n is a scaling constant, equal to 2/3 if $Re < 1$ and 1/2 if $Re > 1$, k is the Von Karman constant, equal to 0.4 in CESM, z_b is the height of the lowest atmospheric layer in the model, u_* is the friction velocity, Sc is the Schmidt number, Re is the Reynolds number, z_0 is the roughness length, g is gravity, and μ is the kinematic viscosity of air. The quantity M describes the relative importance of turbulent versus molecular transport within the surface layer, and comes from the work of *Brutsaeart* [1975a, 1975b].

The isotopic evapotranspiration fluxes from land are computed in a similar manner, but also accounting for evaporation from soils, intercepted canopy water, and snowpack, as well as transpiration, and is described in detail in a separate study [*Wong et al.*, 2017]. Isotopic evaporative fluxes associated with sea ice, on the other hand, are assumed to be nonfractionating, which is similar to previous modeling studies [e.g., *Lee et al.*, 2007].

2.2. Moist Convection

In CAM5, moist convection is split into deep convection [*Zhang and Macfarlane*, 1995] and shallow convection [*Park and Bretherton*, 2009]. The convective schemes are quite different from each other in terms of their physical processes and assumptions, and the water isotopologues are designed such that they experience the same convective transport that standard water vapor and condensate experience in each of these separate parameterizations. However, the phase changes that occur in these convective schemes are similar enough that the impact of these changes on water isotope ratios can be parameterized consistently.

The water vapor isotopic tendency for the deep convection [*Zhang and Macfarlane, 1995*] in grid cells containing clouds is:

$$\frac{\partial q_i}{\partial t} = E_i - C_i - \frac{1}{\rho}\frac{\partial}{\partial z}\left(M_u q_{iu} + M_d q_{id} - M_c q_i\right) \tag{11}$$

where q_i is the normalized isotopic specific humidity, E_i is the evaporation of isotopic cloud condensate (including precipitation), C_i is the isotopic condensation rate, q_{iu} is the isotopic vapor in the updraft, q_{id} is the isotopic vapor in the downdraft, M_u is the updraft mass flux, M_d is the downdraft mass flux, M_c is the net convective mass flux, and ρ is the density of air. A similar mass balance equation is written for cloud condensate. Below cloud base, the water vapor isotopic tendency is:

$$\frac{\partial q_i}{\partial t} = -\frac{1}{z_b - z_s}\left(M_b\left(\left(q_i(z_b) - \mathrm{q}_{iu}(z_b)\right) + M_d\left(q(z_b) - q_{id}(z_b)\right)\right)\right) \tag{12}$$

where z_b is the height of the cloud base, z_s is the surface height, and M_b is the cloud base mass flux. The conversion of cloud condensate to precipitation occurs within the updraft, while downdrafts remain at

saturation via the evaporation of falling precipitation. Evaporation of precipitation into environmental air is handled separately as discussed below.

The water vapor isotopic tendency for the shallow convection [*Park and Bretherton*, 2009] is:

$$\frac{\partial q_i}{\partial t} = -g\frac{\partial}{\partial p}\left(M(qt_i - qt_{ie}) + M_{pen}\left(qt_{ipen} - qt_{ie}\right)\right) - P_i + E_{pi} - \frac{\partial L_i}{\partial t} - \frac{\partial I_i}{\partial t} \tag{13}$$

where M is the convective mass flux, M_{pen} is the penetrative entrainment mass flux, L_i is the isotopic cloud liquid, I_i is the isotopic cloud ice, q_{ti} is the total isotopic water specific humidity in the cloud ($q_i + L_i + I_i$), q_{tie} is the total environmental isotopic water specific humidity, P_i is the production of isotopic precipitation, and E_{pi} is the reevaporation of isotopic precipitation. The cloud liquid and ice tendencies include both advection and detrainment, which are nonfractionating, as well as phase changes to and from water vapor, which produce an isotopic fractionation.

Below the freezing level (0°C), for both schemes, cloud liquid is formed via condensation, and it is assumed that all cloud liquid is in isotopic equilibrium with the remaining water vapor. The new equilibrated isotopic specific humidities are calculated during the formation of the condensate using the method:

$$q_i = (q_{i0} + L_{i0}) * \frac{1}{\left(\frac{\alpha_e}{\Gamma - 1}\right) + 1}, \quad \Gamma = \frac{q}{q + L} \tag{14}$$

$$L_i = L_{i0} - (q_i - q_{i0}) \tag{15}$$

where q_i is the equilibrated isotopic water vapor, L_i is the equilibrated isotopic cloud liquid in specific humidity units, q_{i0} is the isotopic water vapor pre-equilibration, L_{i0} is the isotopic cloud liquid preequilibration, q is the standard model water vapor, L is the standard model cloud liquid, and α_e is the equilibrium fractionation factor.

Whenever cloud ice is formed, either when the updraft is fully glaciated or in the case of mix-phased clouds, it is assumed to deposit directly from vapor. During this process the isotopic water is assumed to undergo Rayleigh distillation, such that the final isotopic vapor and ice masses are solved for using these equations:

$$q_i = q_{i0}\left(\frac{q}{q_0}\right)^{\alpha_{ki}} \tag{16}$$

$$I_i = I_{i0} - (q_i - q_{i0}) \tag{17}$$

where q_i is the isotopic vapor mixing ratio after condensation, I_i is the isotopic cloud ice mixing ratio after condensation, q_{i0} is the isotopic vapor pre-distillation, I_{i0} is the isotopic ice predistillation, q is the standard model water vapor, q_0 is the water vapor specific humidity before ice formation, and α_{ki} is the total (equilibrium plus kinetic) fractionation factor for vapor depositing onto ice:

$$\alpha_{ki} = \frac{\alpha_e S}{\alpha_e \frac{D}{D_i}(S - 1) + 1} \tag{18}$$

where α_e is the equilibrium fractionation factor and S is the supersaturation, which is essentially how much the relative humidity is greater than one, or 100% [*Jouzel and Merlivat*, 1984]. In the model, the supersaturation is parameterized using the equation:

$$S = A_s + B_s * (T - T_{zero}) \tag{19}$$

where T is the temperature in Kelvin, T_{zero} is the triple point for freshwater, which in the model is equal to 273.16 K, and A_s and B_s are parameters which must be selected [*Jouzel and Merlivat*, 1984]. Here we use values of $A_s = 1.0$ and $B_s = -0.002$, which were tuned in order to match the observed precipitation d-excess over Antarctica, with d-excess defined as:

$$d = \delta D - 8 * \delta^{18}O \tag{20}$$

while the shallow convection scheme manages cloud liquid and ice independently, the deep convective scheme uses a bulk condensate method. In order to separate liquid and ice in deep convection, a liquid/ice fraction variable is calculated based on temperature:

$$v = \frac{268.15 - T}{30} \tag{21}$$

where v is the liquid/ice fraction of condensate, and T is the temperature in Kelvin, with v limited to be between zero and one. If the temperature is above 268.15 K then all of the condensate is assumed to be liquid ($v = 0$), while if the temperature is below 238.15 K then all of the condensate is assumed to be ice ($v = 1$). The same liquid/ice fraction formulation is used in the CAM5 macrophysics [*Park et al*., 2014] to determine the fraction of ice and liquid in detrained convective condensate. This formulation assumes that all liquid or ice is formed directly from vapor condensation/deposition, and currently does not allow for other microphysical processes, such as the Wagner-Bergeron-Findeison process, which needs to be treated as a special case.

There is also one phase change, the evaporation of precipitation in near-saturated in-cloud downdrafts produced by the deep convection, where we follow the approach of *Kurita et al*. [2011] and assume that no fractionation occurs. This is equivalent to assuming that the vapor starts off in (near) isotopic equilibration with the rain drops, and that the evaporative fluxes come from the complete evaporation of small drops, which is an assumption that warrants further investigation in future work.

Finally, any phase change also causes latent heating or cooling, which changes the air temperature and in turn the fractionation factor. Therefore, the temperature of fractionation is chosen to be the arithmetic mean temperature during the time step, including the air temperature before and after latent energy changes.

2.3. Stratiform Cloud Physics

Stratiform cloud physics is split into two parameterizations to separately handle the macrophysics [*Park et al*., 2014], which calculates the grid-scale condensation and cloud fraction, and the microphysics [*Morrison and Gettelman*, 2008], which calculates all of the subgrid scale processes occurring internally in the cloud. Both of these parameterizations have similar-enough aspects that they can be grouped together for the purposes of discussing their impact on water isotope ratios.

All cloud liquid condensate that is formed is kept in isotopic equilibrium with the vapor under the assumption that the equilibration time scale for cloud-size droplets is shorter than the typical model time step of 15–30 min, and ice formed from vapor experiences a Rayleigh distillation with an accompanying kinetic fractionation. All processes that generate rain or snow from existing condensate (autoconversion, accretion, collection, and sedimentation) occur with no fractionation. Similarly there is no fractionation during the freezing or melting of condensate. Figure 1 shows all of the reservoirs of water in the cloud physics routines, and the processes that move mass between them. All of the processes that produce a fractionation in the water isotope ratios are shown in red.

The Wagner-Bergeron-Findeison (WBF) process is treated explicitly within the isotopic scheme despite the underlying formulation in CAM5 that treats the process as a direct transfer of liquid to cloud ice or snow. *Gedzelman et al*. [1994] similarly pointed out the need for special attention in treating the isotopic exchanges of the WBF process in bulk microphysical models. This is because the WBF processes involve phase changes from liquid to vapor, and then from vapor to ice, which generates isotopic fractionation. Thus, the WBF process for water isotopologues is modeled simultaneously as an evaporation of cloud liquid, an equilibration of cloud liquid and water vapor, and then a deposition, and isotopic distillation, of the isotopologue vapor onto cloud ice.

Each time step condensate sedimentation is modeled as an advective processes, with a subsequent adjustment to account for evaporation or sublimation of condensate that falls into a clear sky region. Since the evaporation is assumed to involve the complete removal of cloud droplets, there is no accompanying fractionation. The remaining isotopic cloud liquid and vapor are then isotopically equilibrated to account for the addition of new liquid or vapor at each vertical level. Finally, the temperature used to calculate the fractionation factors is an average between the temperatures before and after phase changes occurs.

2.4. Isotopic Exchange During Rain Evaporation

Rain evaporation produces a fractionation for both the rain mass itself and the vapor receiving the evaporated moisture [*Stewart*, 1975], which can have a substantial impact on the global distribution of water isotope ratios [*Risi et al*., 2008]. In CAM5, rain evaporation occurs in both the deep and shallow convective

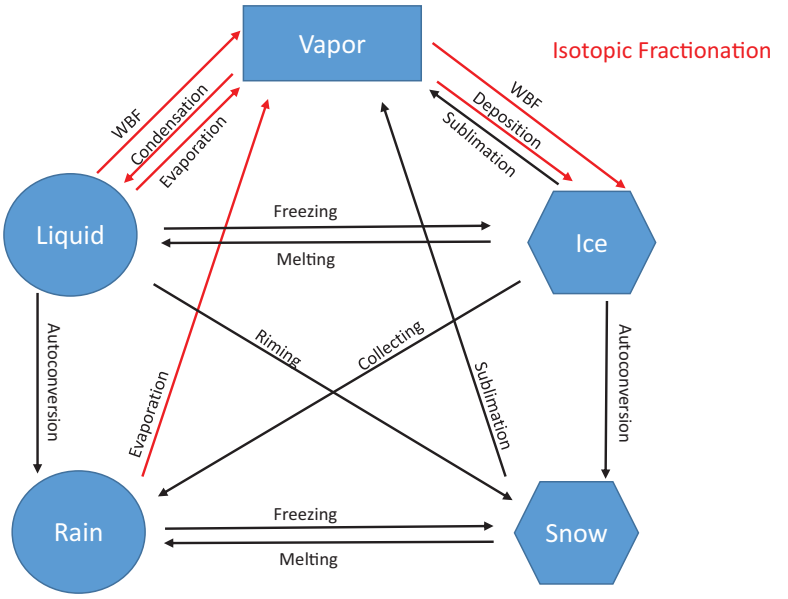

Figure 1. Depiction of microphysical processes accounted for in CAM5. The blue shapes represent all of the physical states of water and water isotopologues allowed in the cloud physics schemes. The arrows indicate physical processes that convert between the different states of water, with the red arrows being processes that produce isotopic fractionation.

schemes, and in the large-scale microphysics. The scheme developed for iCAM5 follows *Stewart* [1975] and is formulated similarly to the scheme described by *Lee et al*. [2007] and *Lee and Fung* [2008] for CAM2.

Precipitation from convective and large-scale clouds is tracked downward as it falls, and evaporates if it encounters a subsaturated layer. The isotope ratio of a drop tends toward a fully equilibrated state relative to the ambient water vapor along the drop's path. However, this isotopic equilibration may be incomplete if the drop is large and the atmospheric layer the drop is falling through is shallow. Thus, often-times a "partial" equilibration occurs, with only a fraction of the raindrop's mass experiencing full equilibration. The magnitude of this partial fractionation is calculated as the ratio between the time needed for the raindrop to equilibrate if the ambient air is saturated, and the time needed for the raindrop to fall through the atmospheric layer of interest. The isotopologue-specific e-folding equilibration time given by *Stewart* [1975] and *Lee and Fung* [2008] is:

$$\tau_e = \frac{\alpha_e r^2 \rho_{H_2O} R_{H_2O} T}{3 f_v D_{ia} e_s} \tag{22}$$

Here α_e is the equilibrium fractionation factor, r is the raindrop radius (m), ρ_{H_2O} is the density of liquid water (kg m^{-3}), R_{H_2O} is the gas constant for water vapor (J K^{-1} kg^{-1}), T is the air temperature (K), D_{ia} is the diffusivity of isotopic water vapor through air (m^2 s^{-1}), e_s is the saturation vapor pressure (Pa) at temperature T, and f_v is a ventilation factor calculated as:

$$f_v = \begin{cases} 0.78 + 0.308 * x, & x \geq 1.4 \\ 1 + 0.108 * x^2, & x < 1.4 \end{cases} \tag{23}$$

$$x = Re^{1/2} Sc^{1/3} \tag{24}$$

where Re is the Reynold's number and Sc is the Schmidt number, and the formula itself is from *Pruppacher and Klett* [1997]. The Reynolds and Schmidt numbers themselves are calculated as:

$$Re = \frac{2 r \rho V_{rain}}{\mu} \tag{25}$$

$$Sc = \frac{\mu}{\rho D_{ia}} \tag{26}$$

where ρ is the density of air, V_{rain} is the vertical fall velocity of the rain drop (described below), and μ is the viscosity of air in kg m^{-1} s^{-1}, calculated as:

$$\mu = (1.72 * 10^{-5}) \left(\frac{T}{273}\right)^{1.5} \left(\frac{393}{T+120}\right) \tag{27}$$

Equation (27) comes from *Rodgers and Yau* [1989], while equations (25) and (26) come from *Pruppacher and Klett* [1997]. Finally, the diffusion of isotopic water vapor through air is calculated as:

$$D_{ia} = (2.11 * 10^{-5}) \left(\frac{D}{Di}\right) \left(\frac{T}{273.15}\right)^{1.94} \left(\frac{101325}{P}\right) \tag{28}$$

where P is the air pressure in Pa, as shown in *Pruppacher and Klett* [1997].

The time scale for the drop to fall through a vertical layer is calculated as:

$$\Delta z = z_{top} - z_{bottom} \tag{29}$$

$$\tau_f = \frac{\Delta z}{V_{rain}} \tag{30}$$

where z_{top} is the altitude for the top of the atmospheric layer in m, z_{bottom} is the altitude for the bottom of the atmospheric layer in m, and V_{rain} is the raindrop fall velocity in m/s. The fall velocity is assumed to equal the terminal velocity, resulting from the balance of gravitational acceleration and non-linear drag [e.g., *Straka*, 2009], which is:

$$V_{rain} = V_{terminal} = \sqrt{\frac{4}{3} \frac{2gr\rho_{H_2O}}{C_d \rho_a}} \tag{31}$$

where g is gravity, r is the raindrop radius, ρ_{H_2O} is the density of liquid water, ρ_a is the density of air, and C_d is the drag coefficient, set to be 0.6 [*Straka*, 2009]. The raindrop radius itself is assumed to be the mass-weighted average based off the rain rate, and it is assumed that the raindrop size distribution follows a Marshall-Palmer distribution [*Marshall and Palmer*, 1948]. The raindrop radius can be derived following the equation of *Williams and Gage* [2009] and is found to be:

$$r = \frac{0.002}{4.1\beta^{-0.21}} \tag{32}$$

where β is the rain rate in units of mm/h, with the denominator as a whole being unitless and the numerator being in units of meters. Finally, the fraction equilibrated is calculated to be an exponential approach to complete equilibration using the ratio of the two time scales:

$$f_e = 1 - e^{-\frac{\tau_f}{\tau_e}} \tag{33}$$

This results in the final equilibrated specific humidity values being equal to:

$$q_i = (1 - f_e) q_{i0} + f_e q_{ie} \tag{34}$$

where q_i is the final isotopologue specific humidity (for either water vapor or rain), q_{i0} is the preequilibrated specific humidity, and q_{ie} is the isotopic vapor if the system is in isotopic equilibrium with the precipitation (see equations (14) and (15), where L and L_i are rain water and isotopic rain water, respectively). This almost always occurs when the relative humidity is 100%. This formulation is consistent with that given by *Stewart* [1975] in delta notation, when the surrounding environmental air is at a high relative humidity and thus likely to be equilibrating. A kinetic effect is also captured in our formulation through the difference in D_{ia} and thus τ_e and f_e for the different isotopologues, although this is not the same kinetic process as described in *Stewart* [1975], which applies only to subsaturated conditions. This formulation is attractive in that the strength of the fractionation is directly dependent on the rain rate. Thus, the influence of drop size, which is a function of the rain rate and allowed to be different for each rain event, can now be captured.

However, one issue with using a partial equilibration method like this one is that it may not be able to capture the correct isotopic response in situations where rain is evaporating into very dry environments. In those situations, the isotopic response should be more like a Rayleigh distillation, with a kinetic fractionation effect that decreases the *d*-excess in precipitation. This process can be captured in the original *Stewart* [1975] formulation, but may not be properly simulated if one is always assuming at least some equilibration,

as is done with the above formulation. To examine this issue, sensitivity tests were performed where the isotopic tendencies due to rain evaporation for convective precipitation were calculated using the original *Stewart* [1975] parameterization. The results of these tests are discussed in section 4.

2.5. Model Configuration

An isotope-enabled CAM5 control simulation was run for the years 1975–2014, with output from January 1979 onward being examined in order to avoid spin-up issues. The model uses a finite-volume dynamical core with a horizontal resolution of 1.9° N × 2.5° E, and a hybrid sigma/pressure vertical coordinate system with 30 vertical levels that increase in thickness with height up to 3 hPa. The model is coupled to an isotope-enabled land model (iCLM4) for land-surface processes [*Wong et al.*, 2017], an isotope-enabled sea ice model (iCICE4) for sea-ice processes (although with prescribed sea ice coverage, thickness, and isotope ratios), and prescribed sea surface temperatures for the ocean [*Hurrell et al.*, 2008]. Ocean isotope ratios are assumed to be constant in time but vary in space, with a *d*-excess of zero, based off the ocean oxygen isotope data set of *LeGrande and Schmidt* [2006]. All other boundary conditions are based off historical data through 2005, with a combination of observations and RCP4.5 scenario emissions from 2005 to 2014 [*Lamarque et al.*, 2010, 2011; *Meinshausen et al.*, 2011].

3. Model Results

3.1. Base Climatology of iCAM5

Figure 2 shows the zonally averaged model results for specific humidity and temperature for the years 1979–2014, and their differences when compared to ERA-Interim [*Dee et al.*, 2011]. It can be seen that compared to the reanalysis, the model has higher specific humidity (typically +0.23 g/kg) and lower temperature (−1.59 K). Figure 3 shows the average precipitation and surface evaporation fluxes over that same time period, along with the differences compared to ERA-Interim. The global bias in precipitation is +0.13 mm/d, although most of the positive bias occurs over the ocean, with large negative biases in some tropical land regions, including the Amazon and Congo. There is also a large positive evaporative flux bias, particularly over the subtropical oceans. The bias when averaged over the globe is +0.16 mm/d compared to ERA-interim. It should be noted that these biases are not a product of adding water isotopes to CAM5, but are instead biases that exist in the underlying nonisotopic atmospheric model. The difference in the precipitation and evaporation bias may indicate that the model was not fully spun-up at the beginning of the analysis, or that the model may not be perfectly conserving water mass.

A physical consistency between these fields would suggest that some of these biases are simply a response to others. For example, if there is an error in the surface evaporative flux such that it adds too much moisture to the atmosphere, then the precipitation increase could simply be a response to the additional mass and higher relative humidity. On the other hand, if the convection and cloud parameterizations generate too much precipitation, then the surface moisture flux bias may simply be a response to the drying of the atmosphere. Water isotopologues can help distinguish between these possibilities, and requires careful assessment of the biases in simulated water isotopologue values.

3.2. Isotope Ratios in the Simulated Water Cycle

Figure 4 shows the annual December–January–February (DJF) and June–July–August (JJA) average δ^{18}O and *d*-excess of precipitation from iCAM5 averaged over the years 1980–2014, compared against stations from the Global Network of Isotopes in Precipitation (GNIP) [*International Atomic Energy Agency* (*IAEA*), 2016]. Only stations with at least two full years of data were used, which resulted in a total of 276 stations available for comparison. An additional seven stations were added from studies in the Maritime Continent region as well, in order to improve the spatial coverage of isotopic precipitation stations globally [*Kurita et al.*, 2009; *Moerman et al.*, 2013]. The model is generally depleted everywhere in terms of δ^{18}O, with a global average bias of $-2.57‰$, while the bias for δD is $-20.03‰$ (not shown). This bias is similar to the results from *Lee et al.* [2007], which found a depleted bias in the older CAM2, particularly for Africa and Asia. The model also has *d*-excess values that are too high (global average bias = $+3.25‰$), although the sign of the local bias varies by region. The majority of GNIP stations are in Europe, so comparisons are naturally weighted towards Northern Hemisphere midlatitude land. However, these isotopic biases have similar values even if the European stations are ignored (not shown).

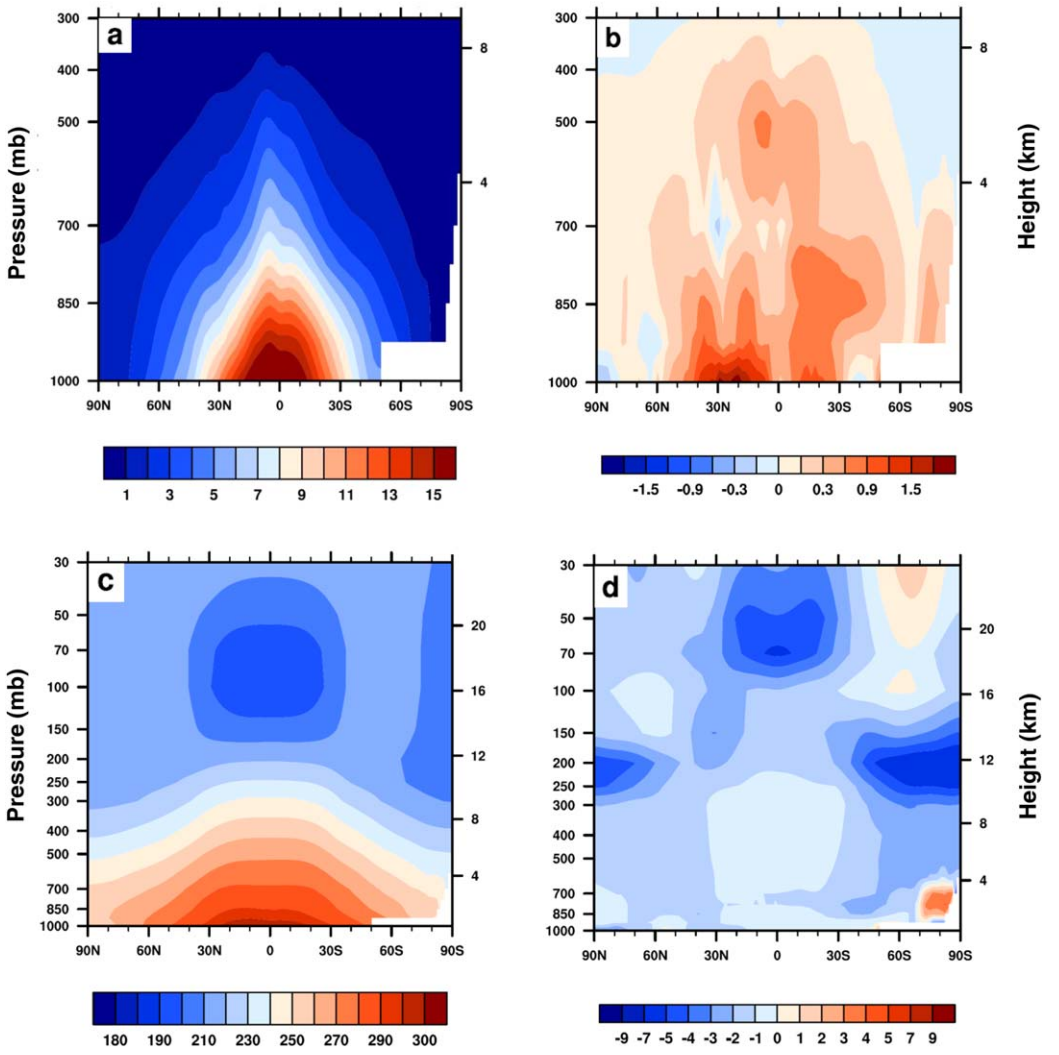

Figure 2. (a) Annual mean zonally averaged specific humidity in g/kg and (c) temperature in K as simulated by CAM5 for 1979–2014, and (b) the difference between the model and ERA-Interim in terms of specific humidity in g/kg and (d) temperature in K.

To help visualize these differences, a scatterplot of the annual average iCAM5 δ^{18}O and *d*-excess in precipitation colocated and compared against the GNIP observations is shown in Figure 5. The red circles represent the control simulation, while the black line represents the values iCAM5 would have if it exactly matched GNIP. It can be seen that for δ^{18}O (Figures 5a and 5c) most of the values are below the line, indicating that iCAM5 is too depleted relative to GNIP, except down near the most depleted GNIP values, where iCAM5 becomes more enriched. For *d*-excess (Figures 5b and 5d), iCAM5 is almost always above the line, indicating *d*-excess values that are too positive compared to GNIP. It can also be seen that the iCAM5 values have a much more uniform distribution, indicating that the spatial variations in *d*-excess are not as large as those seen in the observations. These *d*-excess biases may be at least partially explained by the use of a fractional equilibration scheme for rain evaporation, which may not produce the kinetic fractionation expected for rain drops evaporating in a low relative humidity environment as predicted by *Stewart* [1975].

One concern when using climate or earth system models is whether the horizontal resolution is adequate to capture the features of interest. In order to evaluate the impact of resolution, two additional experiments were conducted for the years 1995–2014, with the first 5 years ignored for spin-up. The first run, labeled "1 × 1" has a 0.9°N × 1.25°E resolution, which is double the control run's resolution. The second run, labeled "0.5 × 0.5," has a 0.47°N × 0.63°E resolution, which is double that of the 1 × 1 run. The annual average

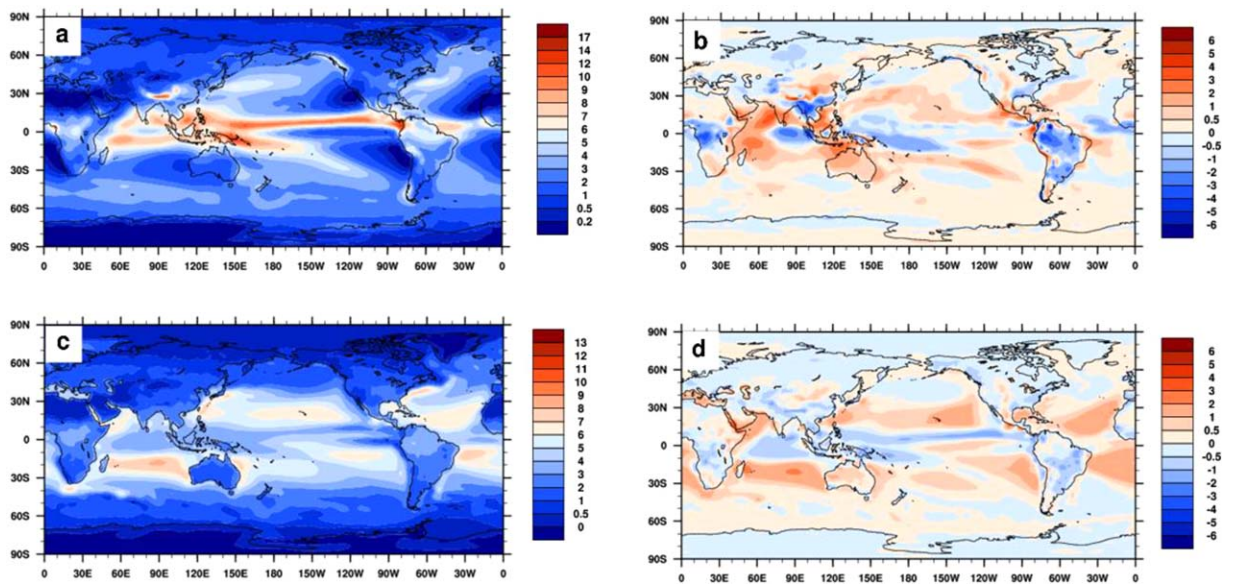

Figure 3. (a) The long-term annual average precipitation rate and (c) surface evaporation flux as simulated by iCAM5 for 1979–2014, and (b) the difference between the model and ERA-Interim in terms of precipitation and (d) surface latent heat flux. The units are in mm/d.

δ^{18}O of precipitation for each of these runs, along with difference between the higher resolution runs and the control ("2 × 2") run, is shown in Figure 6. It can be seen that although some regions, particularly in the high-latitudes, improve, most likely due to better-simulated topography and the ability to begin to resolve some mesoscale circulation features, the overall global bias remains the same. In fact, the annual average δ^{18}O precipitation bias is the same within two decimal places for all three simulations, at a value of $-2.45‰$. These results can also be seen in Figures 5c and 5d, where the green and purple circles represent the higher resolution iCAM5 runs. Thus, the global bias seen in precipitation isotope ratios is not just a result of low resolution, but instead related to the physics of the model itself. However, it should again be noted

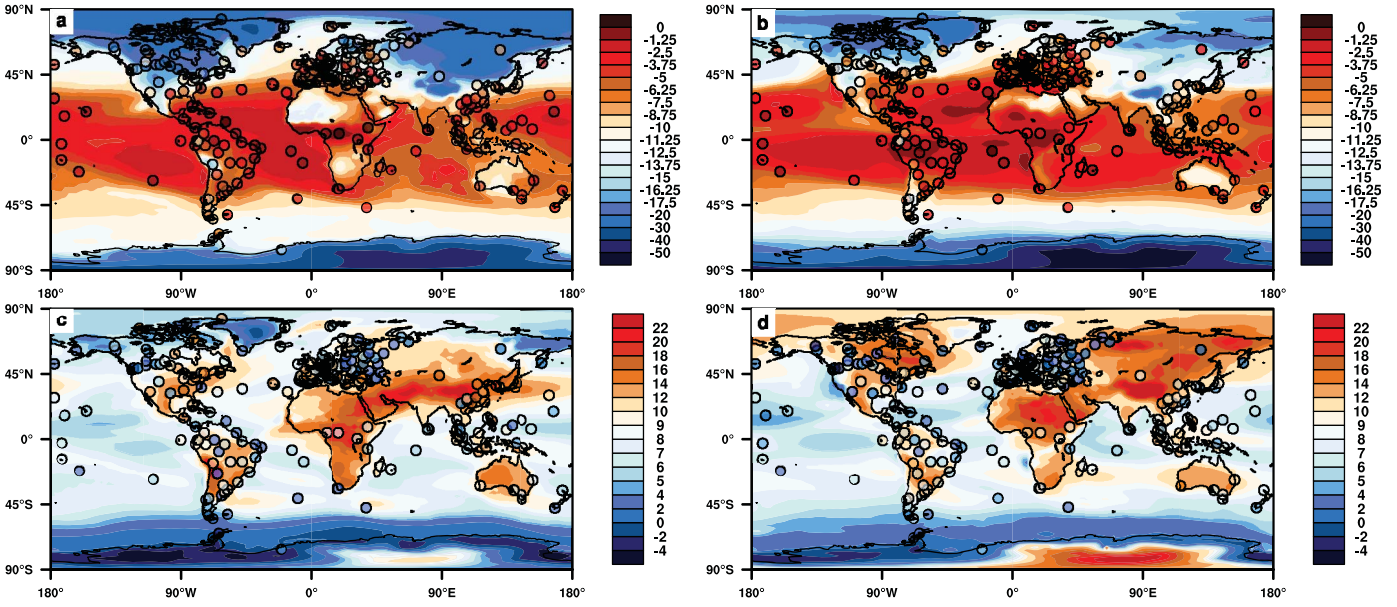

Figure 4. (a) The long-term average δ^{18}O of precipitation in DJF and (b) JJA, and the long-term average *d*-excess of precipitation for (c) DJF and (d) JJA, as simulated by isotope-enabled CAM5 for the years 1980–2014. The circles indicate GNIP stations, with the colors of the circles indicating the respective long-term average δ^{18}O or *d*-excess of precipitation measured at that site using the same color scale as the contours. For δ^{18}O, the contours increase by $10‰$ up to $-20.0‰$, then jump to $-17.5‰$ and increase by $1.25‰$ afterward. For the *d*-excess, the contours increase by $2‰$ up to $+4‰$, then increase by $1‰$ up to $+10‰$, after which they again increase by $2‰$.

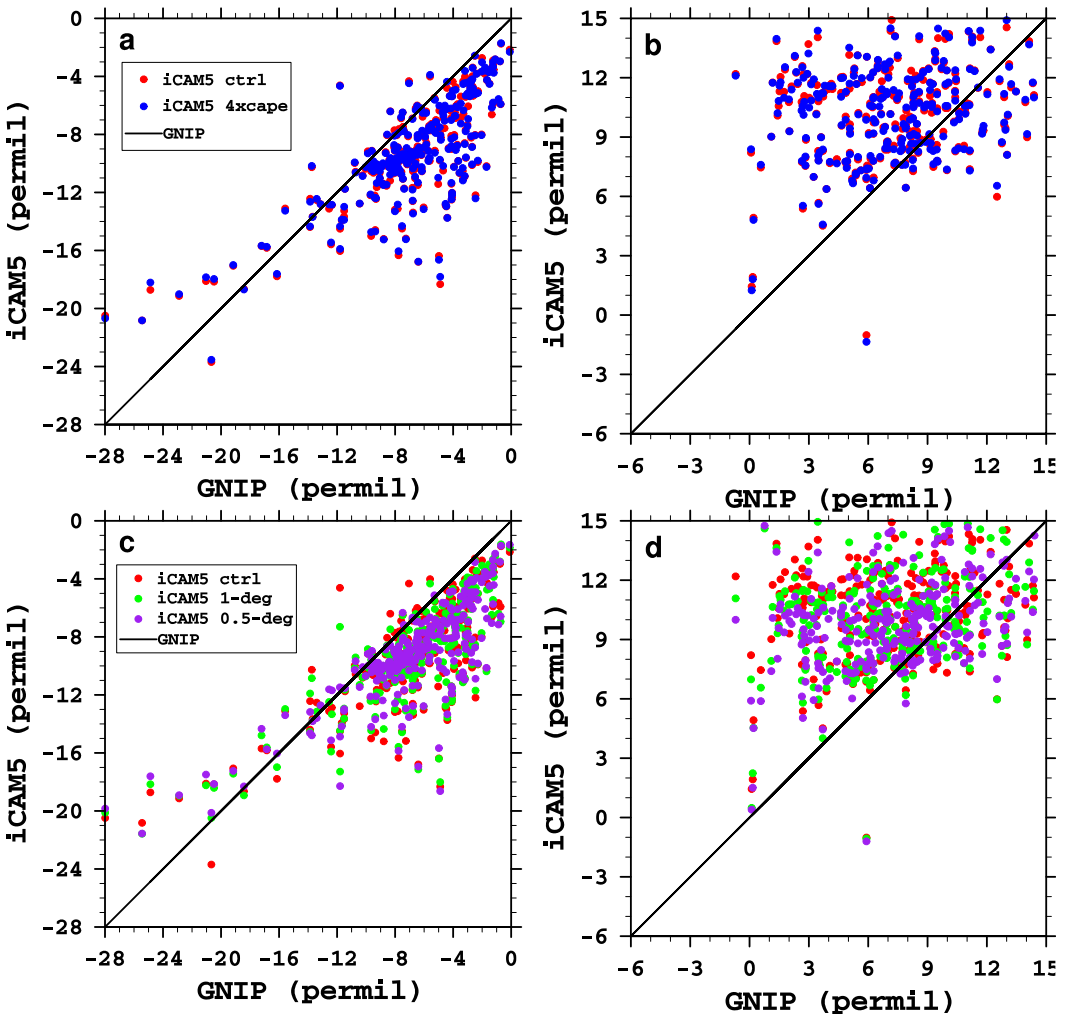

Figure 5. (a and c) A scatter plot comparing the annual average GNIP values for $\delta_{18}O$ in precipitation and (c and d) *d*-excess in precipitation (c and d) against the colocated annual averaged values as simulated by iCAM5. The red circles are for the iCAM5 control (2 × 2) run, the blue circles are for the iCAM5 run with the increased deep convective CAPE trigger (4xcape), the green circles are for the iCAM5 1 × 1 run, and the purple circles are for the iCAM5 0.5 × 0.5 run. The black diagonal line represents an exact fit between the observations and model values.

that this is only true on the global scale, as specific regions experience very large changes in the isotopic ratios at different resolutions, particularly at the "0.5 × 0.5" resolution.

Figure 7 shows the average clear-sky vertical column-integrated δD of vapor as simulated by iCAM5 for the years 2003–2007, and the average difference between the model and column-integrated δD as measured by SCIAMACHY [*Frankenberg et al.*, 2009; *Scheepmaker et al.*, 2013]. The dates were chosen in order to match the time period of the SCIAMACHY observations, although the model was not specifically sampled on the satellite trajectory, which could generate errors purely due to temporal or spatial sampling differences. The SCIAMACHY results are also not absolutely calibrated, which could also introduce observational errors and biases [*Frankenberg et al.*, 2009]. The simulation results show isotope ratios that are lower than observations throughout the tropics, but higher than observations in the extratropics. This results in a global average bias of $-9.76‰$, which is likely within the uncertainty of the observations, assuming a precision of 15% for the SCIAMACHY observations [*Frankenberg et al.*, 2009]. However, comparisons against ground-based remote-sensing observations have shown a depleted bias in the SCIAMACHY results [*Scheepmaker et al.*, 2015]. Thus, even if the iCAM5 results matched up perfectly with SCIAMACHY, this would still indicate a depleted bias, at least for the tropics and subtropics. This demonstrates that the depleted bias is present in water vapor as well as precipitation, and that the precipitation bias is not purely due to the isotopic

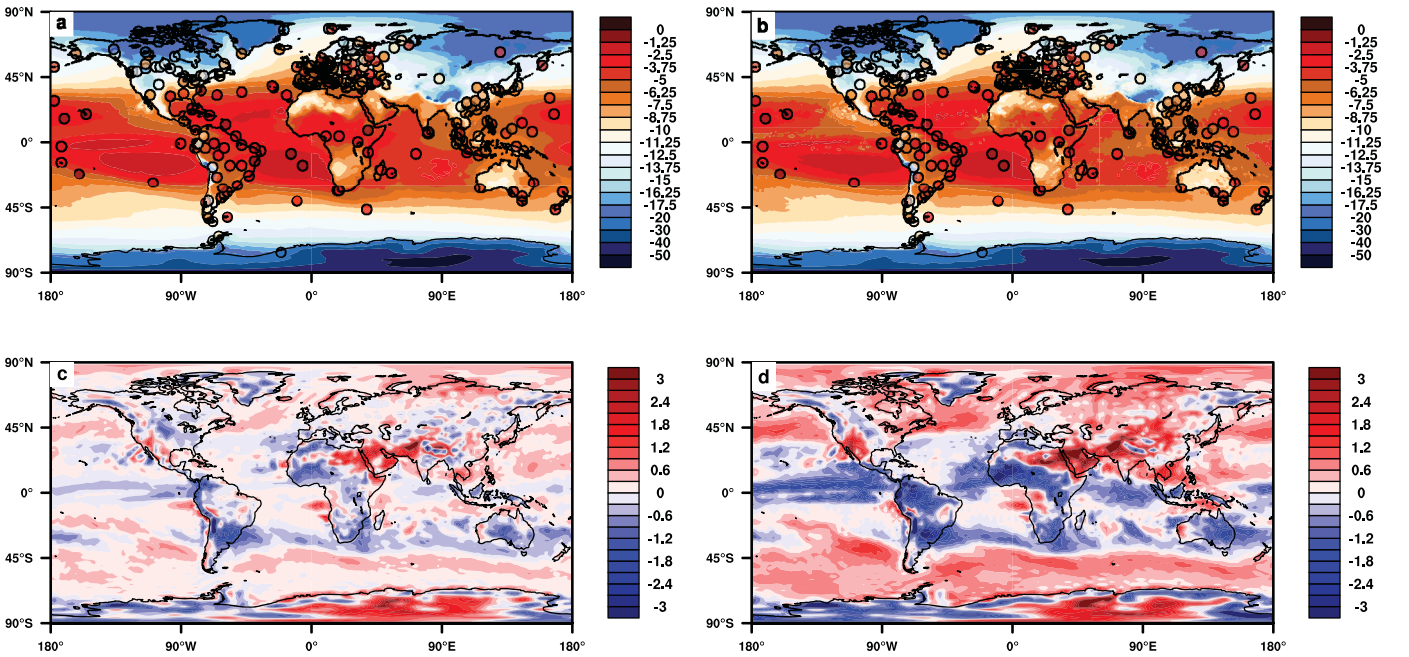

Figure 6. Maps of the long-term annual average $\delta^{18}O$ of precipitation for a simulation at: (a) 0.9°N × 1.25°E ("1 × 1") resolution, and (b) 0.47°N × 0.67°E ("0.5 × 0.5") resolution, along with the annual average from the GNIP stations (colored circles). The contours are the same as Figure 4 for $\delta^{18}O$. (c) Also shown is the difference in the annual average $\delta^{18}O$ of precipitation between the 1 × 1 simulation and the control simulation, and (d) the difference between the 0.5 × 0.5 simulation and the control simulation. The higher-resolution simulations were re-gridded to the control run grid in order to allow for a direct comparison. The units are in permil (‰).

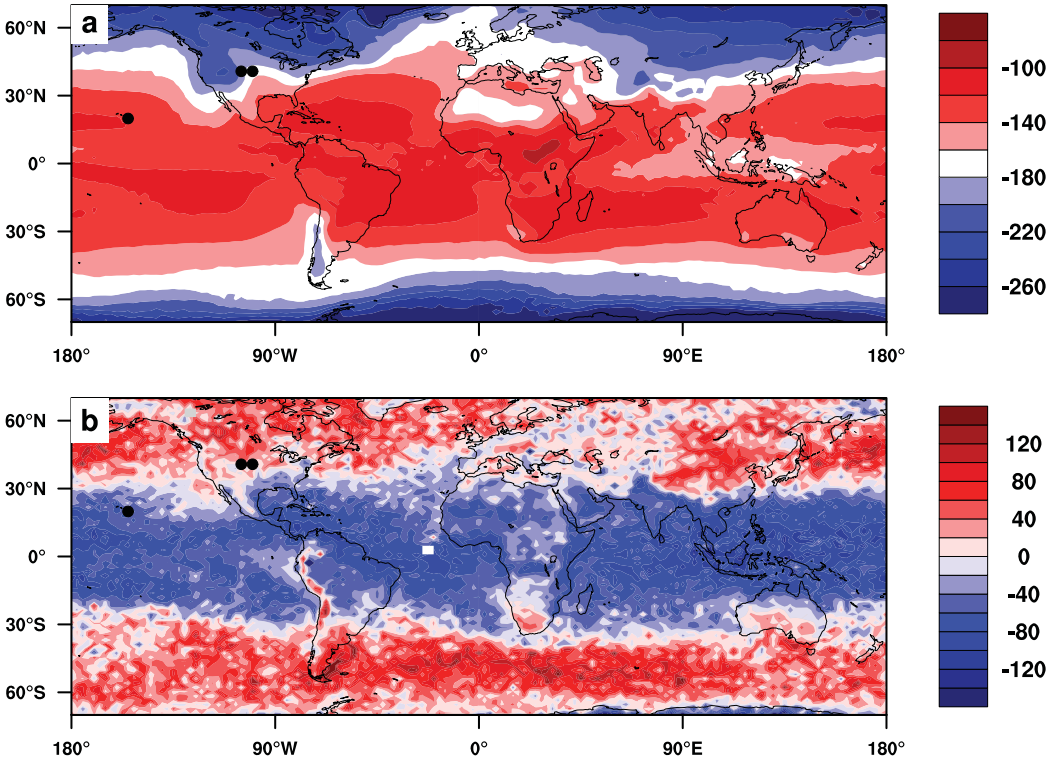

Figure 7. (a) The vertically integrated average δD in permil of water vapor as simulated by iCAM5 for the years 2003–2007, and (b) the difference between the model and SCIAMACHY in permil, averaged over the same time period. The black circles mark the locations of the Colorado and Hawaii isotopic surface vapor measurement locations, with the Greenland station being too far north to be matched up with the satellite data.

fractionation schemes in clouds. Still, it should be stated that other comparisons against SCIAMACHY have indicated that the satellite data might have an enriched bias [*Frankenberg et al*., 2013], and so the actual values provided by SCIAMACHY are quite uncertain. Finally, it should also be noted that the latitudinal gradient in the simulated vertically integrated δD is too flat, which is similar to other isotope-enabled GCM results [*Yoshimura et al*., 2011; *Risi et al*., 2012a].

To more closely examine the vapor, Figure 8 shows the average simulated surface vapor δD and *d*-excess for each month at four point locations for each model resolution, along with monthly average measurements as provided by in situ laser spectrometers. The four locations are Niwot Ridge, CO [*Berkelhammer et al*., 2016], Erie, CO, Mauna Loa, HI [*Bailey et al*., 2015b], and Summit, Greenland [*Bailey et al*., 2015a], although the instrument in Greenland had some technical issues during July of each year, which could put the observations during that time into doubt. The vertical solid lines indicate one standard error range for the measurements.

For the different climate zones sampled by these sites, CAM5 shows general agreement in the shape of the seasonal cycle for δD, but the magnitude is too small, particularly for Niwot Ridge. This result is not significantly improved by model resolution, at least for the resolutions examined here. The model is also, on average, enriched in δD compared to observations, which is opposite that of the precipitation bias. However, most of these locations are in the extratropics, where SCIAMACHY also showed an enriched vapor bias (the locations of all stations except Summit are marked by the black circles in Figure 7). The out-of-phase, or lagged, relationship seen between the model and observations in Mauna Loa has been seen in other GCMs for the subtropics as well [*Risi et al*., 2012a]. For *d*-excess, the model does not capture the seasonality in any location except possibly Summit, and is generally biased high in the midlatitude stations, and biased low in the subtropical and polar stations. It is possible that some of these errors are coming from the way the water isotopes are treated in the land-surface model during evapotranspiration [*Wong et al*., 2017], but future work will be needed to explore these biases fully. Finally, it is important to note that both Mauna Loa and Niwot Ridge are elevated in height relative to their surroundings (each are $\sim$3000 m a.s.l), and thus do not necessarily represent the actual atmospheric surface layer. Niwot Ridge, CO and Erie, CO are also only separated by $\sim$60 km, which can be smaller than the length scale of the model grid box, especially at the lower resolution control (2×2) run. Nonetheless, iCAM5 at all resolutions satisfyingly captures the early summer maximum observed at Niwot Ridge that is not observed (or modeled) at Erie, where the summer isotope ratio maximum is shorter in duration.

Given that precipitation mass is sourced from atmospheric water vapor, the negative δD bias in the integrated water vapor should impart (and thus explain) some of the δD bias in precipitation. However, the specific cause of the vapor bias has yet to be determined: there either must be too little isotopologue mass being evaporated or transpired into the atmosphere, or too much isotopologue mass must rain out during transport, particularly over regions where there is sparse coverage in the GNIP database (such as over the ocean). To our knowledge, there are no systematic, or even point wise, observations of isotopic evaporative flux over the open ocean that can offer a direct comparison with the CAM5 modeled isotopic evaporative flux.

3.3. Diagnosis of Biases in Water Transport

To help identify if the isotope ratios of the evaporative flux are responsible, near-surface vapor (which if depleted would indicate depleted surface fluxes), is compared to water vapor above the boundary layer (indicating rain-out if erroneously depleted). Figure 9 shows the δD for vapor at the lowest model layer, and the difference between the model and the interpolated surface data from *Good et al*. [2015], which used a combination of Tropospheric Emission Spectrometer (TES) retrievals [*Worden et al*., 2006] and surface observations to generate an estimate of low-level vapor δD. The average for the model was calculated using output for the months for which a sufficient volume of TES observations were available (September 2004 to May 2011, excluding June 2005, January 2010, and February 2010). We focus on oceanic regions where the observations are of higher quality, and thus the possible influence of remote land sources should be borne in mind. Outside of the maritime continent, the model is enriched relative to the *Good et al*. [2015] marine boundary layer vapor δD climatology, with a global average bias of $+9.87‰$, which is greater than the average observational uncertainty of $2.9‰$. This indicates that isotopic surface fluxes, at least from the ocean, are most likely not the cause of the global precipitation bias.

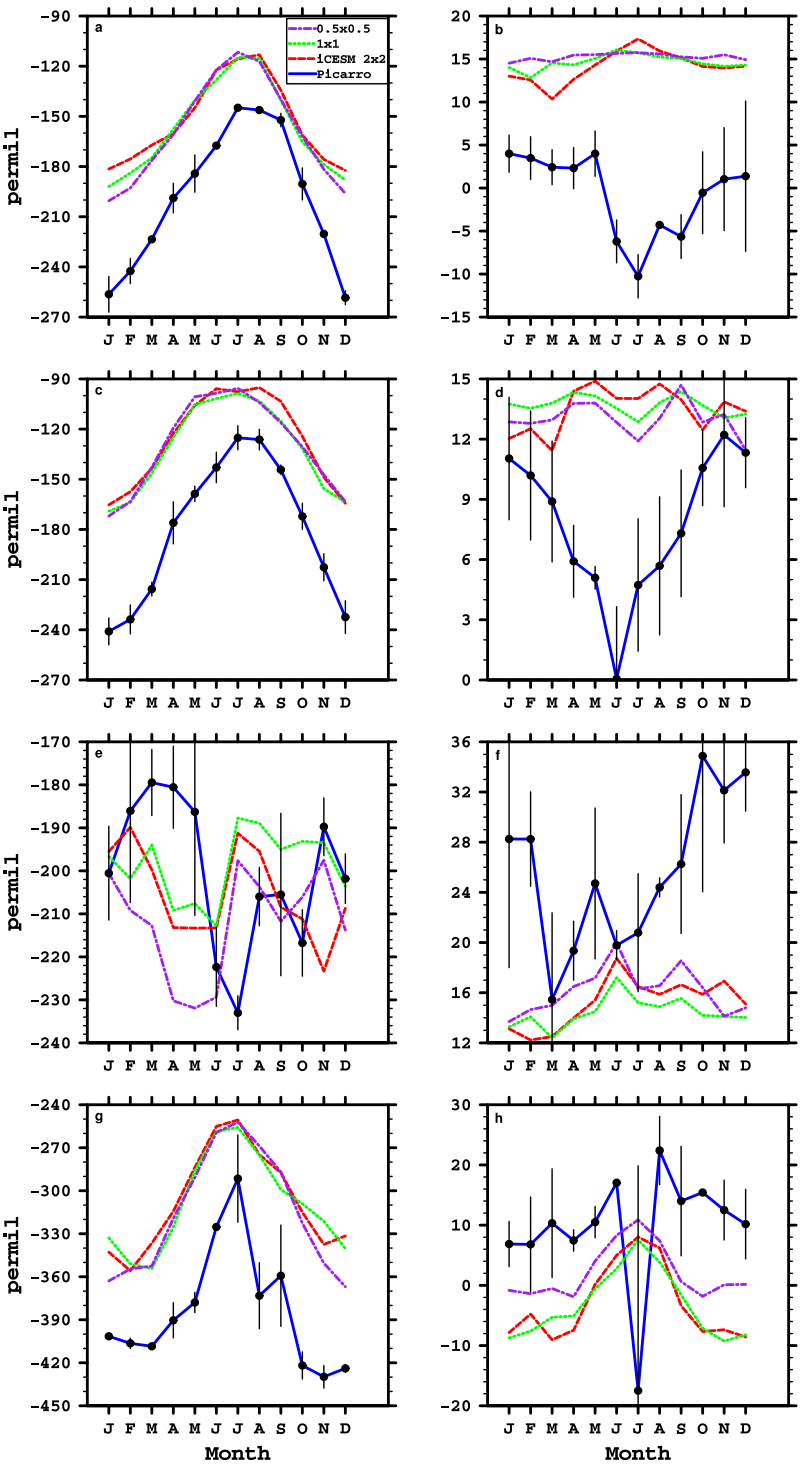

Figure 8. The monthly average surface vapor δD in permil as simulated by CAM5 at three different resolutions (2 × 2—red dashed line, 1 × 1—green dashed line, and 0.5 × 0.5—purple dashed line), and as measured by a Picarro spectrometer (blue solid line) for: (a) Niwot Ridge, CO, (c) Erie, CO, (e) Mauna Loa, HI, and (g) Summit, Greenland, along with the average surface vapor *d*-excess for: (b) Niwot Ridge, CO, (d) Erie, CO, (f) Mauna Loa, HI, and (h) Summit, Greenland. The vertical black lines represent ±1 SE for the Picarro measurements. Finally, please note that the d-excess for July at Summit (plot h) is associated with very low sampling in that month, and thus the July observations may not be representative of the mean.

Figure 10 shows simulated vapor δD over the same time period as Figure 9, but at ∼750 mb, which is close to the top of the boundary layer and the level of maximum TES retrieval sensitivity. It also shows the difference between the vapor δD modeled by iCAM5 and as measured by TES. Given the enhanced sensitivity of

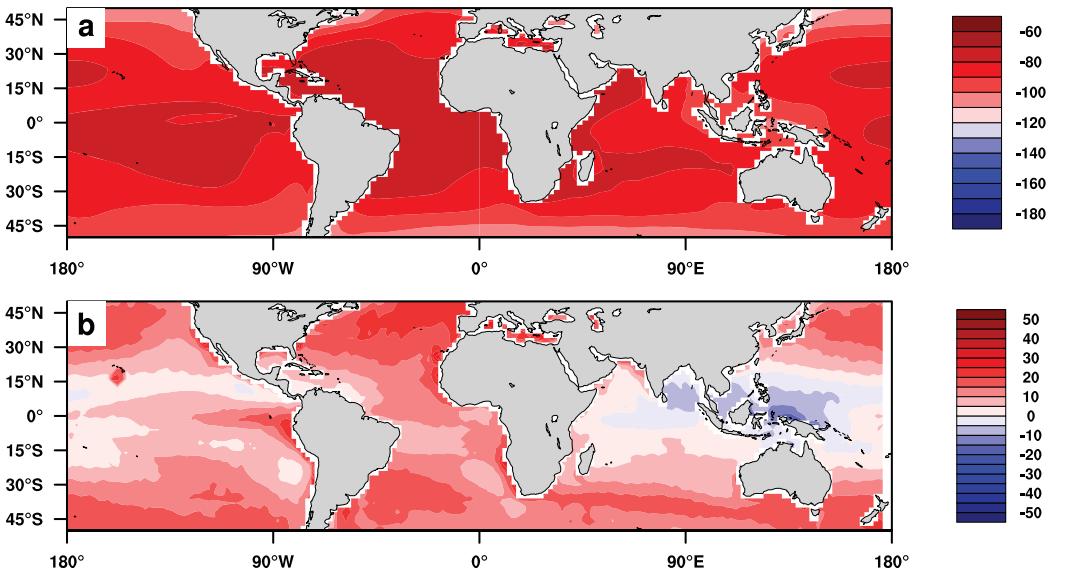

Figure 9. (a) The water vapor δD in permil at the lowest atmospheric model layer in iCAM5, averaged over September 2004 to May 2011, excluding June 2005, January, 2010, and February 2010, and (b) the difference between the model and the *Good et al.* [2015] water vapor δD climatology.

TES at this vertical level, the direct TES retrievals can be used, as long as the model output is convolved with the TES averaging kernel using the so-called "observational operator" [e.g., *Worden et al.*, 2006; *Jones et al.*, 2009]. The model is depleted almost everywhere, with a global average bias of $-41.40‰$, which is larger than the uncertainty in TES if one assumes that an observational bias of 5% in TES [*Worden et al.*, 2006, 2011] is representative of the overall observational uncertainty. This change in the sign of model bias, from overly enriched near the surface to greatly depleted above the boundary layer, indicates that the isotope ratios of water vapor decrease too quickly in the vertical. The only physical processes that can directly remove water isotopologue mass from the atmosphere once it has left the surface is precipitation. Thus, the water isotopologue data suggest that CAM5 produces too much precipitation as water is lifted upward, or vertically mixed, from the surface to the free troposphere. The use of isotopic information to diagnose the

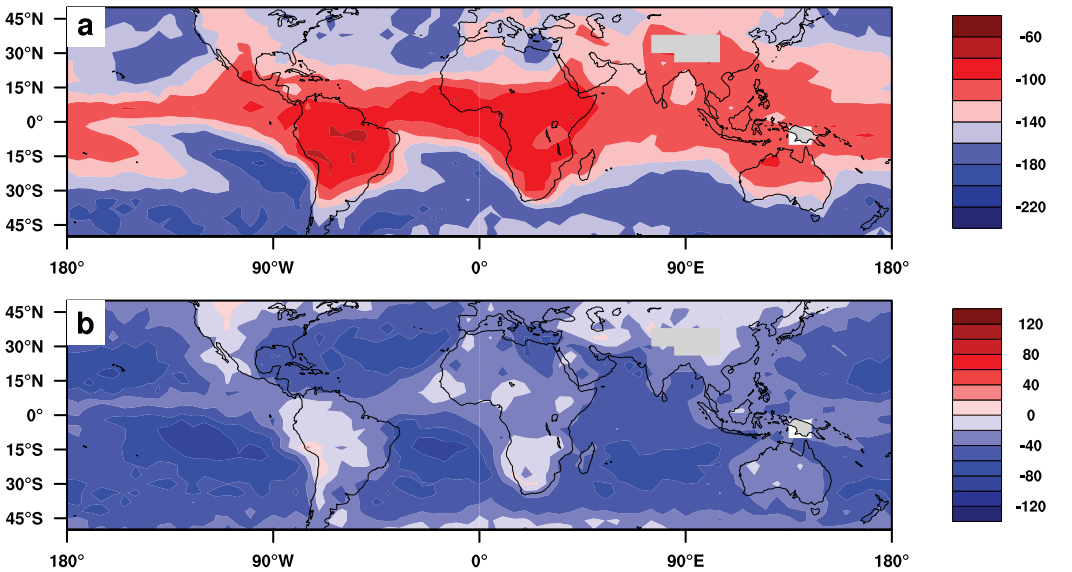

Figure 10. (a) The water vapor δD in permil at ~750 mb in iCAM5, averaged over September 2004 to May 2011, excluding June 2005, January, 2010, and February 2010, and (b) the difference between the model and water vapor δD as measured by TES at the same vertical level and over the same time period.

cause of these biases in the model isotopic partitioning similarly sheds light on the underlying reason for some of the biases in the model's hydrologic cycle.

4. Simulation Sensitivity to Parameter Choice

Model biases in precipitation rates are linked to a set of specific physical processes or parameterizations which have remained difficult to diagnose by conventional means. Given that the isotopic distribution in the atmosphere is strongly influenced by precipitation, it stands to reason that a particular free parameter or set of parameters in the model that influences precipitation could also strongly modify the isotopologue values. This is particularly true for moist convection, which not only produces precipitation, but also transports moisture vertically, particularly from the boundary layer to the free troposphere, where the isotopic bias becomes negative. This will not only help determine the drivers of isotope ratio biases, but also what parameters in the model the water isotopologue values are sensitive to, which aids in determining areas where attention can be placed to achieve future model improvement.

4.1. Overview of Sensitivity Tests

The precipitation in iCAM5 is produced by three different parameterizations, a deep convective scheme [*Zhang and McFarlane*, 1995], a shallow convective scheme [*Park and Bretherton*, 2009], and a large-scale, or stratiform, cloud microphysics scheme [*Morrison and Gettelman*, 2008]. Thus, parameters in each of these schemes were modified in an attempt to reduce either the frequency of precipitation events, or the intensity of precipitation per event, in order to reduce the loss of water isotopologue mass during vertical and horizontal transport. Another possibility outside of clouds and convection is that the nonconvective vertical diffusion in the model, particularly from the boundary layer to the free troposphere, is too weak, resulting in not enough ventilation of moisture from the boundary layer to the free troposphere. To test this possibility, the boundary layers scheme's maximum eddy transport length scale was doubled for one simulation, and halved for another. It is also possible that other convective processes not examined here, like entrainment and detrainment, may also have a noticeable influence, but will be left for future work.

Another set of experiments used different isotopic physics choices, including different fractionation factors. This was done in order to determine to what extent the errors were due to uncertainties in the isotopic physics, as opposed to errors in the modeled hydrologic cycle itself. Two of these experiments where to: A. Replace the *Horita and Wesolowski* [1994] fractionation factors with the more commonly used *Majoube* [1971] factors for liquid/vapor phase changes, and B. Replace the molecular diffusivity ratios of *Merlivat* [1978] with *Cappa et al.* [2003]. This will help determine how uncertainty in the isotopic fractionation factors may influence the model results.

Along with the fractionation factor experiments, two additional experiments replaced the isotopic rain reevaporation parameterization described in this paper with the equations from *Stewart* [1975], specifically:

$$R_s = \gamma R_v + (R_r - \gamma R_v) f^{\beta} \tag{35}$$

$$\gamma = \frac{\alpha_e h}{1 - a_e \left(\frac{D}{D_i}\right)^n (1-h)}, \tag{36}$$

$$\beta = \frac{1 - \alpha_e \left(\frac{D}{D_i}\right)^n (1-h)}{\alpha_e \left(\frac{D}{D_i}\right)^n (1-h)} \tag{37}$$

$$R_s = \frac{r_i}{r} \tag{38}$$

$$R_r = \frac{r_{i0}}{r_0} \tag{39}$$

$$R_v = \frac{q_{i0}}{q_0} \tag{40}$$

$$f = \frac{r}{r_0} \tag{41}$$

$$E_i = r_{i0} - R_s r \tag{42}$$

where r_i is the isotopic rain mass after evaporation, r is the regular rain mass after evaporation, r_{i0} is the isotopic rain mass before evaporation, r_0 is the regular rain mass before evaporation, q_{i0} is the isotopic vapor mass before evaporation, q_0 is the regular vapor mass before evaporation, α_e is the equilibrium fraction factor, D is the diffusivity of regular water, D_i is the diffusivity of isotopic water, n is a scaling constant, set to 0.58 [*Stewart*, 1975], h is the relative humidity, and E_i is the isotopic rain evaporation amount. This was done to examine the importance of the new parameterization scheme used in iCAM5 (equation (340) in determining the role of postcondensation processes on the final isotopic values in rain. This is particularly critical since postcondensational exchange is known to have a strong influence on model results [e.g., *Risi et al*., 2008].

The two experiments also looked at the importance of relative humidity for the *Stewart* [1975] scheme, as it is believed that the standard model parameterization may do poorly in low relative humidity environments. In order to do so, it was assumed that the air near the actual rain mass is more humid than the grid scale average, and so an "effective" relative humidity is used in the Stewart equation instead:

$$h_{eff} = \phi + (1-\phi)h \tag{43}$$

where ϕ is a tunable parameter, equal to $\sim$0.9 in one model experiment, which matches *Bony et al*. [2008], and zero in another model experiment, which means that h_{eff} is simply equal to the grid-scale relative humidity. Also, if the relative humidity is at or near 100%, a singularity in the *Stewart* equations can occur. Thus, whenever the relative humidity is at 100%, the isotopic rain experiences direct equilibration with the vapor, instead of the *Stewart* process. Finally, this parameterization was only applied to the convective precipitation, as it was assumed that the drop sizes in the large-scale precipitation were small enough that they either isotopically equilibrated using the partial equilibration scheme, or evaporated completely.

Finally, two extra experiments were also performed: the first evaluated the assumption that falling rain fully isotopically equilibrates, regardless of the rain intensity or the thickness of the layer through which it is falling. The second experiment artificially raised the temperature used to calculate the equilibrium fractionation factor in the model, to help determine what, if any, impact the temperature bias in iCAM5 has on the simulated isotope ratios.

Table 1 lists the sensitivity experiments that were performed, including the parameter that was modified, and by how much the value was changed. All sensitivity experiments were branched from the control run in the year 1995 and ran until 2014, with the first 5 years ignored for spin-up. This provides 15 years of model output covering the entire isotopologue-measuring satellite era, which permits an examination of isotope ratios in both precipitation and water vapor. It should be noted that while the focus of this analysis is on a single isotope (δD or $\delta^{18}O$), the *d*-excess of precipitation is also shown in Figure 11 to help demonstrate its sensitivity as well.

Figure 11a shows the change in the average bias for each tuning run compared against GNIP (blue). SCIAMACHY (orange), and TES (green), relative to the control run. A value of zero would indicate the simulation has a bias equal to the control run, while a negative value indicates a bias that is more negative relative to the control run (and thus larger in magnitude). The error bars are the 1 SD range of the annual averages from the model. Figure 11b is the same as Figure 11a, except showing changes in the root mean squared error (RMSE) between the model simulations and the observational data sets. The sign of the change in the plot is such that if the change is positive, the RMSE has decreased (or improved) by the displayed amount, while if the change is negative, the RMSE has increased (or worsened) by that amount. If precipitation alone was examined, which was more typical of modeling studies of the past due to a lack of isotopic vapor measurements, one would assume that simply equilibrating rain would produce the best values. However, by examining isotopic vapor data as well it can be seen that completely equilibrating rain produces a very large vapor bias and therefore must be rejected. This is not surprising, given that if a bias exists in precipitation, isotopically equilibrating it with vapor will pass that bias over to the vapor. Thus isotopic postcondensation or rain evaporation schemes should modulate the amount of equilibration or isotopic exchange based on the environmental conditions, such as that which is proposed here in section 2.

Table 1. A List of the Different Tuning Experiments That Were Performed[a]

Run Name	Parameters	Description	Original Value	Modified Value
cldfrc	cldfrc_rhminh	Grid-scale relative humidity needed for high clouds (unitless)	0.8	0.999
cldfrc	cldfrc_rhminl	Grid-scale relative humidity needed for low clouds (unitless)	0.8875	0.999
cldfrc	cldfrc_rhminl_adj_land	The change in the relative humidty cutoff needed for clouds over land (unitless)	0.1	0
dpkevp	zmconv_ke	Rate of sub-cloud rain evaporation for deep scheme ([kg m^{-2} s^{-1}] $^{-1/2}$ s^{-1})	1.0×10^{-6}	2.0×10^{-6}
dpauto	zmconv_c0_lnd	Deep scheme autoconversion rate over land (m^{-1})	0.0059	0.00295
dpauto	zmconv_c0_ocn	Deep scheme autoconversion rate over ocean (m^{-1})	0.045	0.0225
dpcape	capelmt	CAPE needed to trigger deep convection (J/kg)	70	140
3xcape	capelmt	CAPE needed to trigger deep convection (J/kg)	70	210
4xcape	capelmt	CAPE needed to trigger deep convection (J/kg)	70	280
dptau	tau	CAPE consumption time-scale for deep convection (s)	3600	7200
ddmpdz	dmpdz	parcel entrainment rate for CAPE calculation in deep convection (m^{-1})	−0.001	−0.002
shauto	frc_rasn	fraction of condensate from shallow convection that can be converted to precipitation (unitless)	1	0.5
shkevp	kevp	Rate of sub-cloud rain evaporation for shallow scheme ([kg m^{-2} s^{-1}] $^{-1/2}$ s^{-1})	2.0×10^{-6}	4.0×10^{-6}
miauto	micro_mg_dcs	size threshold for autoconversion of cloud ice to snow in large-scale clouds (m)	4.0×10^{-4}	8.0×10^{-4}
2xeddy	eddy_leng_max	Maximum dissipation length scale in PBL scheme (m)	40	80
0.5xeddy	eddy_leng_max	Maximum dissipation length scale in PBL scheme (m)	40	20
raineq	f_e	Isotopic Equilibration fraction for precipitation (unitless)	Variable	1
Teq2K	T_e	Temperature used to calculate equilibrium fractionation factor (K)	Variable	Variable + 2 K
majoube	α_e	Equilibrium fractionation factor (unitless)	Variable	Variable
cappa	D_i/D	Molecular diffusivity ratio between heavy and light water isotopologues (unitless)	Variable	Variable
stew_phi	New parameterization	Use *Stewart* [1975] isotopic rain reevaporation parameterization, with $\varphi = 0.9$	Variable	Variable
stew_rh	New parameterization	Use *Stewart* [1975] isotopic rain reevaporation parameterization, with $\varphi = 0$	Variable	Variable

[a]The run name is the same that is shown in Figure 10. The model parameter name is the name of the free parameter or parameters that were modified for each run, the description explains what each parameter represents, the original value is the default value the parameter has at model set up, and the modified value is what the value was changed to in the run.

The modifications that produce the smallest differences compared to the control run are the changes in some of the convective parameters (dpkevp and dpauto), the maximum eddy length scale (2× eddy and 0.5× eddy), and changes in the fractionation factors and diffusivities (majoube and cappa). This indicates that the biases and errors seen in the simulation are most likely not due to the vertical turbulent diffusion in the model or uncertainties in standard isotopic parameters. It should be noted that much of the vertical mixing is generated through convection, and so the small impact produced by the change in eddy length scale is to be expected. The changes generated by the artificial increase in temperature (Teq2K) also did not appear to produce a major improvement, except possibly in the vapor bias compared against SCIAMACHY. Still, the relatively small improvement indicates that iCAM5's temperature bias is most likely not the main driver of the isotopic errors, at least in terms of modifying the isotopic equilibrium fractionation factors.

One test that produced large changes was the use of the *Stewart* [1975] isotopic rain evaporation scheme with the grid-scale relative humidity. However, the changes were such that large improvements in the vapor were seemingly negated by worsening errors in the precipitation, making it unclear if this method is superior to the partial equilibration method described here. The use of *Stewart* [1975] with an effective humidity, on the other hand, appeared to produce better isotopic ratios, at least for precipitation, indicating that the deficiencies of the partial equilibration scheme in a low-humidity environment are valid, and will be examined more closely in future work. Still, it is important to note that neither of these changes produce improvements large enough to eliminate the annual average bias and RMSE seen in the model, indicating that other, non-isotopic processes in the model are at least partially responsible for generating the errors in the simulated isotope ratios in iCAM5.

All of the remaining parameter tests should modify the distribution of precipitation by decreasing the frequency or intensity or precipitation for certain weather systems. According to these tests, changes to the deep convection resulted in the best comparisons with the observations (see Figure 11). This indicates that the shallow convection and cloud microphysics are either already accurately simulating the processes that impact water isotope ratios, or are tuned as well as possible, at least for the specific parameters examined here. The specific test that produces the greatest improvement in both precipitation and vapor bias and RMSE is when the amount of Convective Available Potential Energy (CAPE) needed to trigger deep convection is increased. This indicates that deep convection is triggered too frequently, which may explain some of the bulk precipitation biases as well as the positive specific humidity bias in the upper troposphere (as

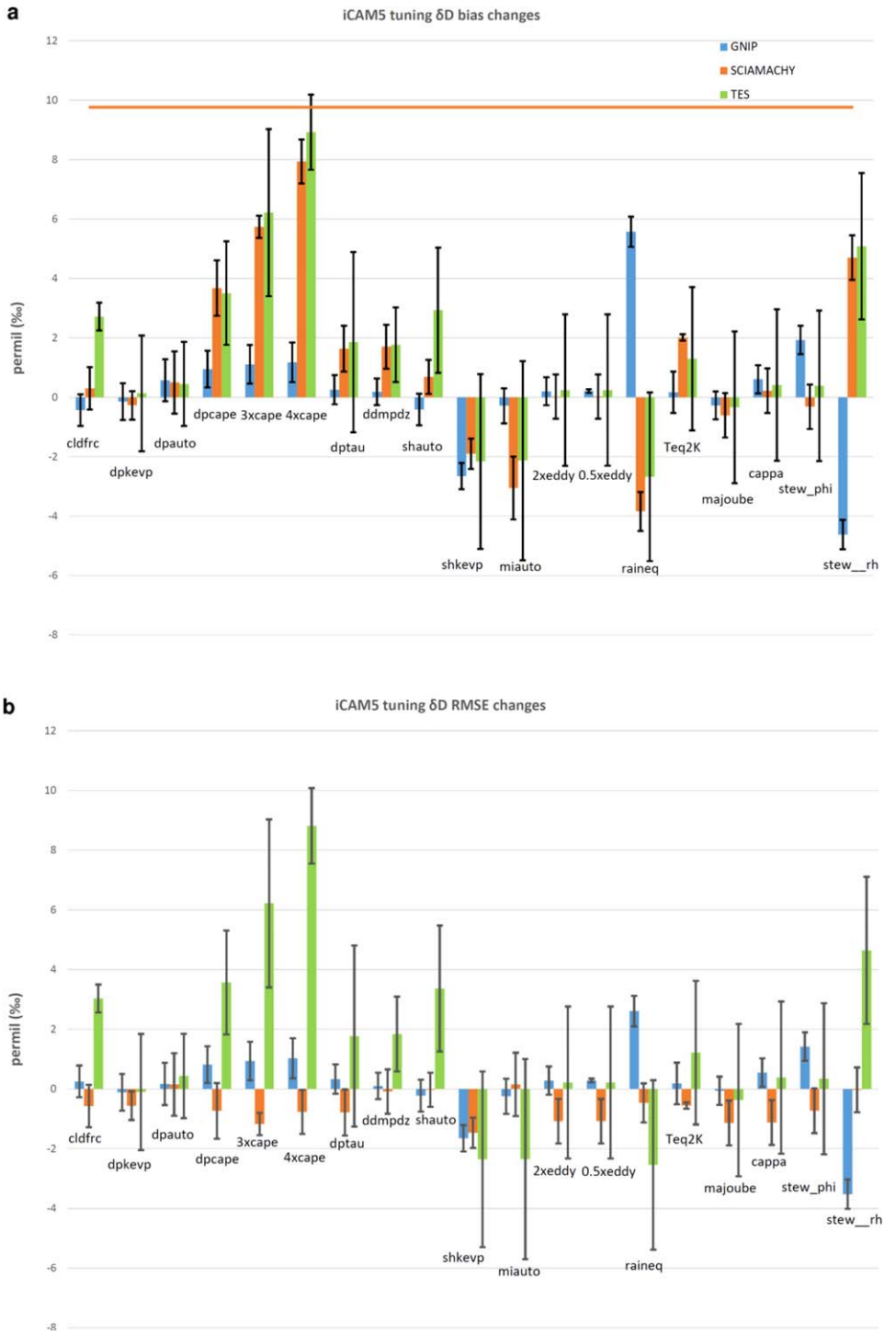

Figure 11. The top plot (a) shows the difference (indicated by the vertical blue bars) in the average δD bias in precipitation in permil as compared to GNIP for the years 2000–2014 for each model run relative to the control run, with a positive bar indicating a smaller bias. The error bars indicate $\pm$SD in the global annual average precipitation δ^{18}O for that particular simulation. The vertical orange bars are the same, except representing the δD bias in integrated water vapor compared against SCIAMACHY, while the vertical green bars are for the δD bias at $\sim$750 mb compared against TEST. The horizontal orange line indicates the change in bias needed to completely remove the global average bias in the SCIAMACHY comparison. The value needed for GNIP and TES are off the chart. All of the simulation names are listed in Table 1. The bottom plot (b) is the same as plot a, except showing the improvement in the Root Mean Square Error (RMSE), with a positive value indicating a smaller RMSE, and a negative value indicating a larger RMSE.

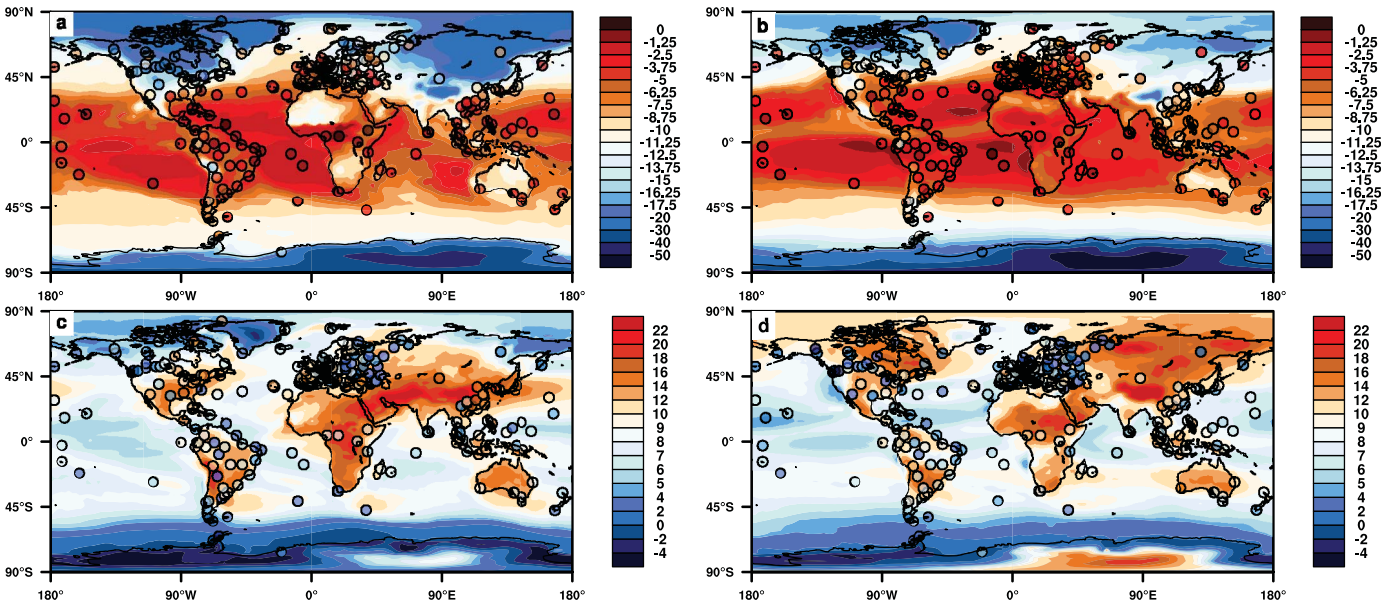

Figure 12. Same as Figure 4, except from the 2 × 2 "4xcape" sensitivity experiment.

deep convection tends to inject moisture into the mid- and upper- troposphere). This finding of a convective trigger threshold that is too weak matches up well with previous studies [e.g. *Xie et al.*, 2004; *Wang and Zhang*, 2013; *Suhas and Zhang*, 2014], indicating that the improvements in the simulated water isotope ratios relate to actual improvements in the model's physical realism. Thus the "4xcape" experiment will be examined more closely to expose the influences of deep convection on the water isotopologue distribution in the model, and to determine to what degree imperfect representation of convective thunderstorms alone can fully explain the isotopic biases seen in iCAM5.

4.2. Increased CAPE Experiment Results

Figures 12 and 13 are similar to Figures 4 and 9, except that the comparison is with the 2 × 2 degree resolution "4xcape" simulation. The δD in vapor shows there is a noticeable global improvement (global bias = $-32.48‰$ versus $-41.40‰$ for the control), particularly in regions where one expects deep

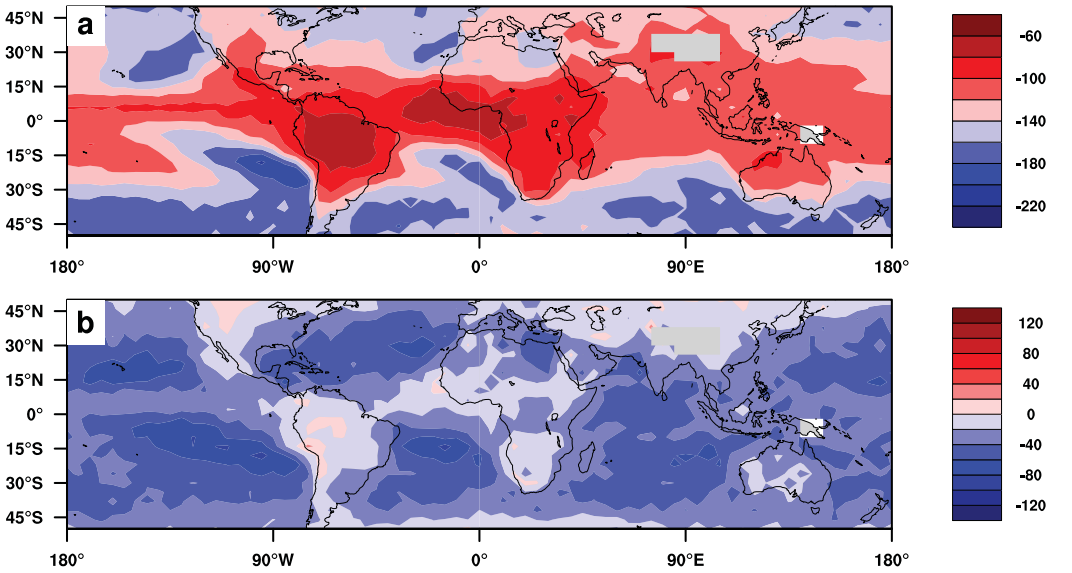

Figure 13. Same as Figure 9, except for the 2 × 2 "4xcape" sensitivity experiment.

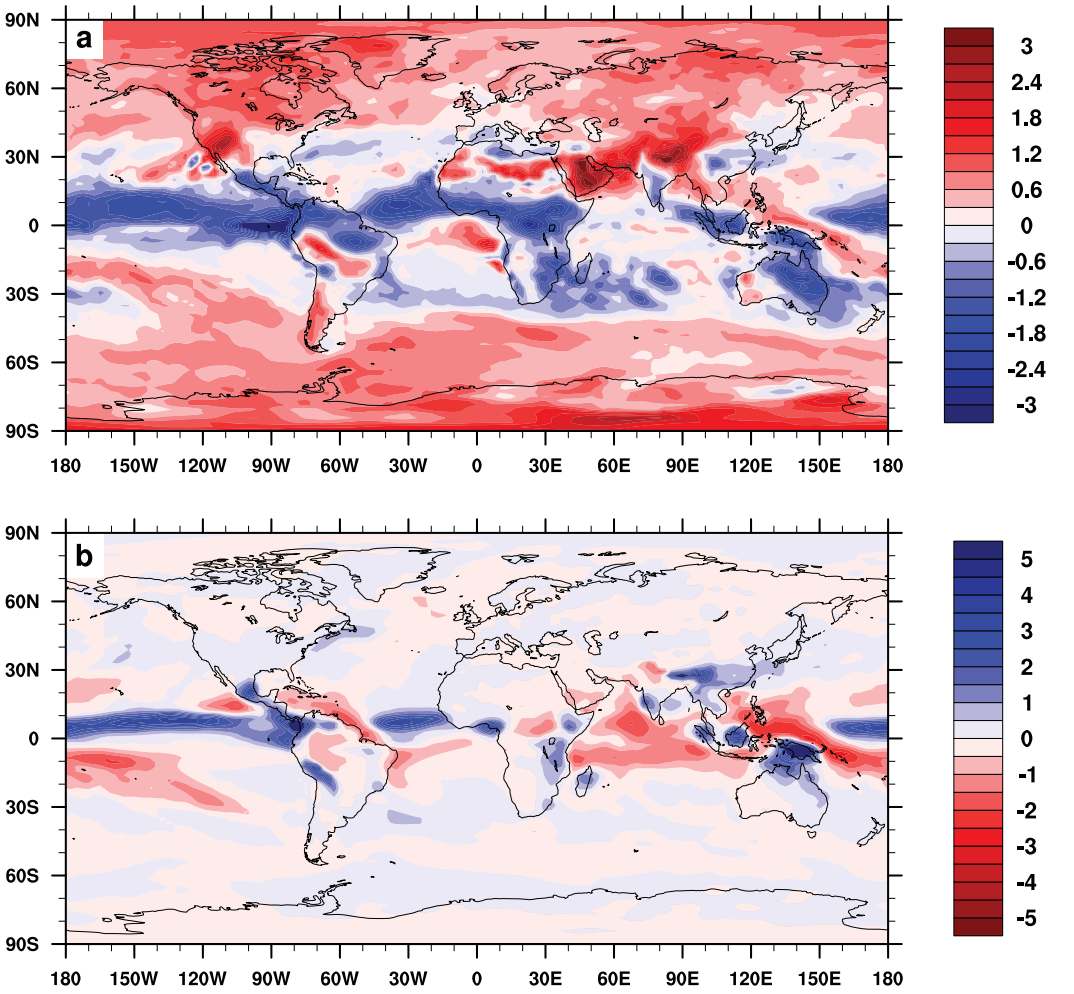

Figure 14. (a) The difference in the δ^{18}O in permil of precipitation between the "4xcape" experiment and the control run, averaged over the years 2000–2014, and (b) the difference between those two runs in terms of average precipitation rate in mm/d over the same time period. Note that color bars are flipped for the two plots (i.e., blue colors indicate more depletion and more precipitation, while red colors indicate more enrichment and less precipitation).

convection to occur, such as in the Inter-Tropical Convergence Zone (ITCZ). However, for δ^{18}O in precipitation the enrichment relative to the control is much less noticeable (global bias $= -2.36‰$), except for in high-latitude regions, which is surprising given that those regions are not locations of frequent or intense deep convection. Thus, it is possible that a larger-scale change in atmospheric circulation or hydrology may be producing the isotopic precipitation changes. Finally, Figures 5a and 5b also show relatively small changes in precipitation isotope ratios compared to the control, except for outliers in the simulated δ^{18}O, which all showed enrichment in the enhanced CAPE simulation (blue circles), and which may be driving the global improvements in bias and RMSE.

To emphasize this point, Figure 14 shows the difference between the "4xcape" run and the control run in δ^{18}O of precipitation (top plot) and in average precipitation rate (bottom plot). A large change in tropical precipitation is evident, which is expected given the prevalence of deep convection in tropical regions. The figure shows that on average the precipitation changes are inversely correlated with the changes in precipitation δ^{18}O. This indicates that the main driver for isotopic precipitation changes in the tropics is the amount effect, which is an observed negative correlation between precipitation amount and the isotopic ratios of the precipitation [e.g., *Dansgaard*, 1964]. However, the actual cause of the amount effect remains unclear [*Lee and Fung*, 2008; *Risi et al.*, 2008; *Moore et al.*, 2014; *Conroy et al.*, 2016]. Outside of the tropics, there is a spatially broad positive difference in the polar and mid-atitude continental regions (see Figure 14a). The change in precipitation amount outside the tropics, though, is

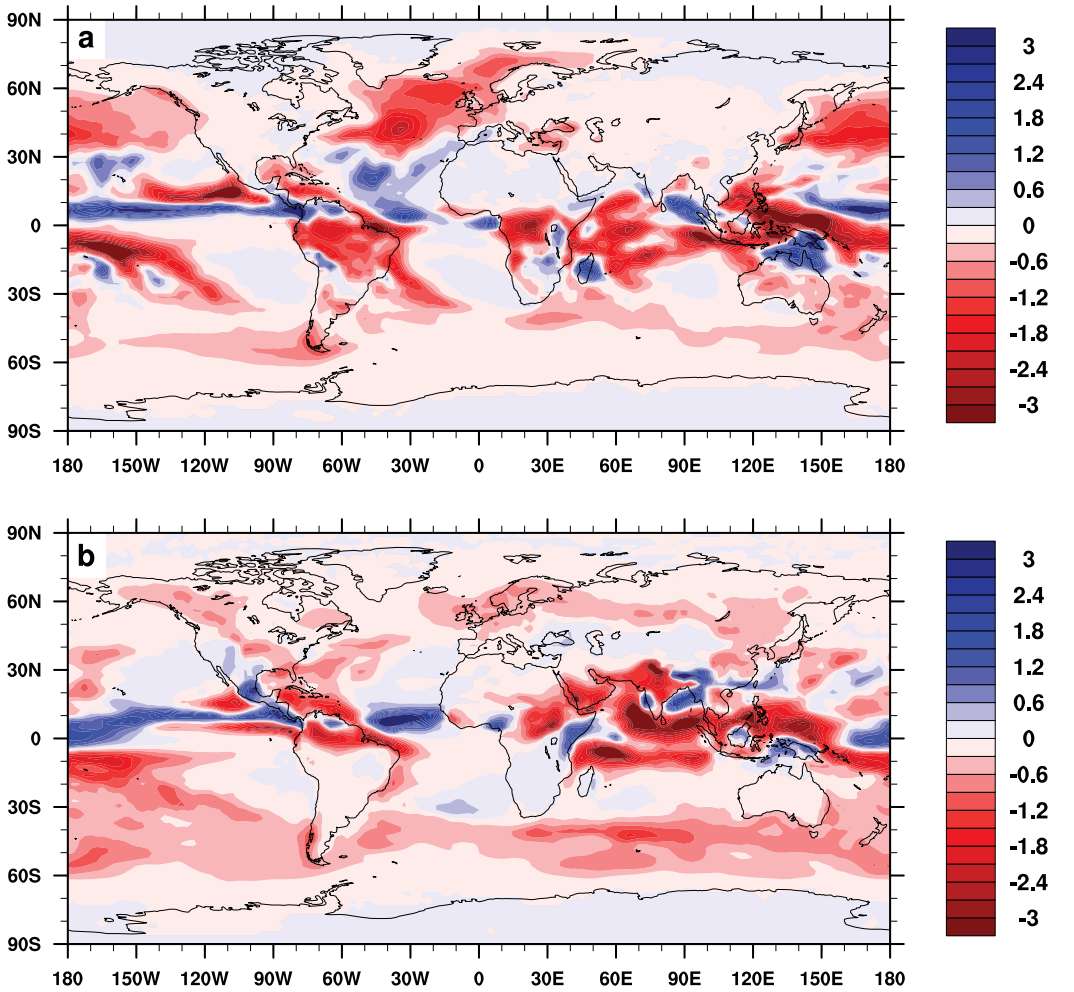

Figure 15. (a) The difference in the average convective precipitation rate between the "4xcape" run and the control run, averaged over December-January–February for the years 2000–2014, and (b) the same difference plot, except averaged over June–July–August. Units are in mm/d.

minimal (Figure 14b). Thus nonlocal processes must be causing the enriched precipitation values, and provides the remarkable insight that lower latitudes exert significant influence on isotope ratios at high latitudes, including over ice sheets.

Although the net precipitation may not change substantially, the amount of precipitation from convection alone does. Figure 15 shows the change in precipitation from convective sources between the "4xcape" and control simulations for DJF (a) and JJA (b). The figure shows that in the midlatitudes the amount of convective precipitation decreases substantially. It can also be seen that this decrease is largest over the oceans in the winter hemisphere, when extratropical cyclones are generating a large amount of poleward moisture transport. By decreasing the removal of isotopic mass from the boundary layer and/or lower troposphere via deep convection in extratropical cyclones, more isotopically enriched water can be transported poleward and landward via the large-scale flow, resulting in more enriched precipitation values in those regions. This indicates that CAM5 is not accurately simulating convective mixing in the atmosphere, which could have a strong influence on global climate sensitivity [*Sherwood et al.*, 2014].

Finally, given that the total precipitation amount did not change substantially, the simulation results indicate that different physical processes are compensating for the decrease in deep convective precipitation. However, both the shallow convection and the resolved vertical flow and large-scale cloud physics tend to not transport moisture upwards as much as the deep convection. This results in water vapor

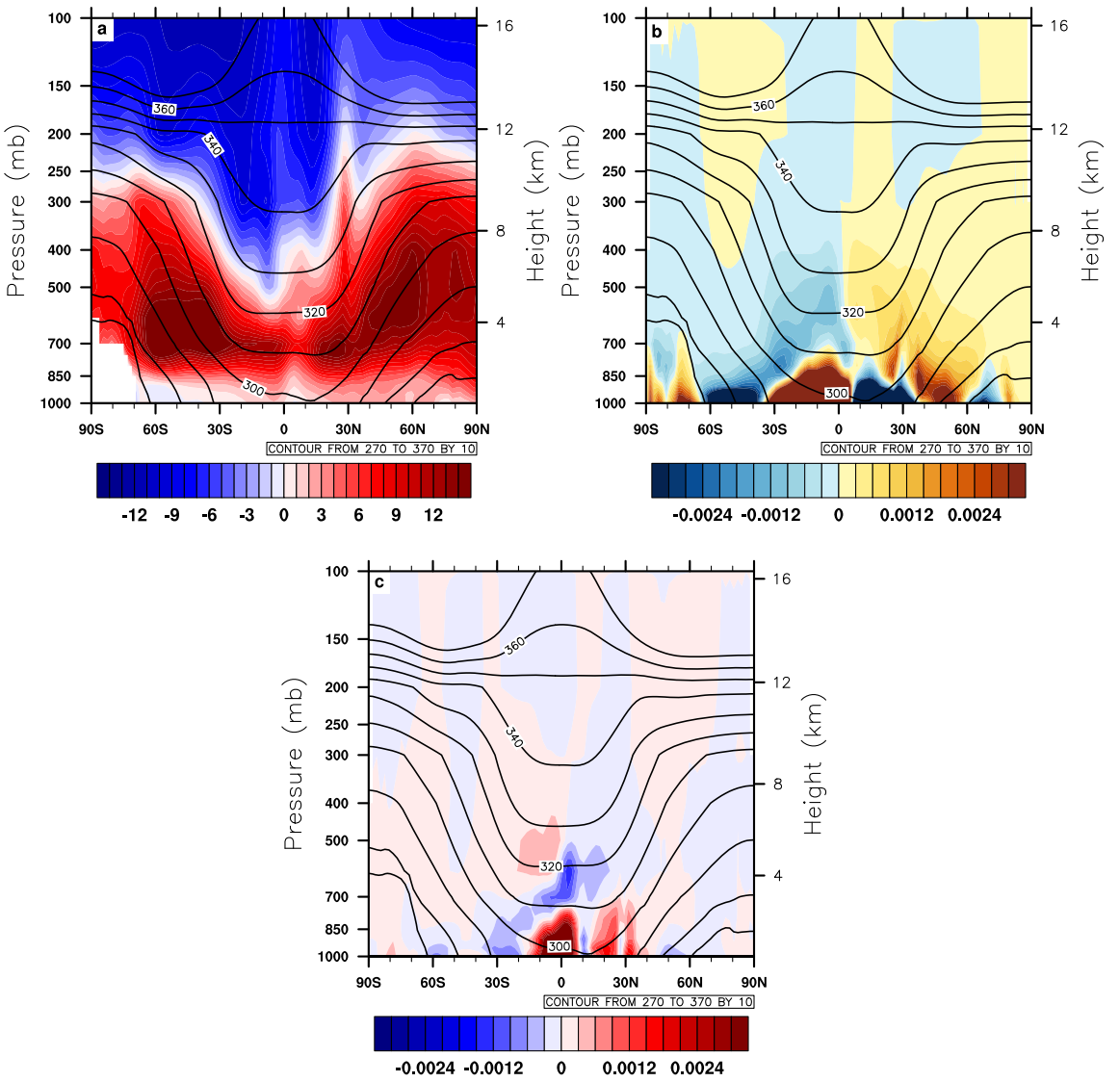

Figure 16. (a) The difference in the zonally averaged water vapor δD in permil between the "4xcape" run and the control run, (b) the average meridional moisture flux (positive = northward) for the control simulation in units of kg m/s, and (c) the difference in the average meridional moisture flux between the "4xcape" run and the control run (c). Also plotted is the zonally averaged potential temperature (black contours) in units of K. All quantities are averaged over the years 2000–2014.

with higher isotope ratios being present in the lower troposphere, as seen in Figure 16, which shows the zonally averaged difference in water vapor δD between the "4xcape" and control simulations (a), along with the zonally averaged meridional moisture flux for the control simulation (b) and the change in the meridional moisture flux between the "4xcape" and control simulations (c). It can be seen that the enriched signal in the "4xcape" run occurs in the same regions as the largest poleward moisture fluxes, indicating enhanced isotopic moisture transport by extratropical cyclones, particularly through the warm conveyor belt, which tends to transport moisture upward from the lower troposphere/boundary layer [*Browning*, 1971]. It can also been seen that the bulk moisture fluxes are not substantially altered outside of the tropics by the changes in convection. This demonstrates that increasing the isotopic ratios of water vapor in the lower troposphere, by decreasing deep convection, has allowed for more effective transport of water isotopologues poleward and landward by the resolved flow, resulting in more enriched precipitation in those regions. Finally, given that this improves the overall isotopic biases, it indicates that the model is, by default, tuned to trigger deep convection more frequently than in nature, especially during winter in the midlatitudes. Therefore future refinements to the *Zhang and McFarlane* [1995] convection scheme in CAM5, or new parameterizations of moist convection, should consider

raising the trigger threshold for deep convection in order to simulate a more accurate hydrologic cycle in the atmosphere of CAM5, and CESM.

5. Conclusions

Simulations of water isotopologues in climate and earth system models enable a wide range of new research possibilities within the fields of paleoclimatology, cloud physics, large-scale hydrology, and land-atmosphere exchange. Many paleoclimate proxy records are based on water isotopologues, so being able to simulate them in a climate model enables the use of proxy system models [*Dee et al*., 2015] and avoids the additional uncertainty brought on by converting the proxy record into temperature or precipitation. Another advantage is that water isotopic data provide an extra constraint on the simulated hydrologic cycle, and can be particularly sensitive to cloud and convective processes, which can be quite poorly constrained otherwise [*Bolot et al*., 2013; *Field et al*., 2014]. This additional information can be used to produce better-tuned models, or even more physically accurate parameterizations.

Water isotopologue physics have been added to the NCAR Community Atmosphere Model Version 5 (CAM5). This isotope-enabled CAM5 (iCAM5) is the latest in a series of isotopic models that follows from other comparable isotope-enabled climate models (e.g., GISS, ECHAM, MIROC, LMDZ), and is capable of simulating the overall isotopic distribution in the atmosphere, including in water vapor and precipitation, with fidelity. Like all models, however, biases and errors were present in a simulation of the modern era, including a large global depleted bias in precipitation as well as a depleted bias in tropical midtropospheric water vapor. Also, the particular isotopic scheme chosen for rain evaporation (partial equilibration) may not produce the correct isotopic response in low humidity environments, and thus generate d-excess values which are too positive. This may explain the high d-excess bias seen in continental precipitation, and will be the focus of future work.

In order to determine causes of the biases in the model hydrological cycle that give rise to the discrepancy between modeled and observed isotope ratios, it was found that the δD in water vapor is overly enriched in the lowest model layer, but quickly becomes more depleted with height. This indicates that CAM5 produces too much precipitation when transporting moisture vertically, and this bias is at least partially independent of the surface evaporative flux. These biases together describe a hydrologic cycle in the model that is characteristically different from nature. This result of precipitation biases in the model producing overly depleted isotope ratios was also found for the older CAM2 [*Lee et al*., 2007], and demonstrates a potential problem in the underlying physics routines common to both models.

In one experiment, precipitation was forced to isotopically equilibrate with the surrounding vapor. Although this improved the isotopic precipitation bias, it greatly increased the bias in water vapor. This shows that with satellite and in situ measurements of water isotopologues in vapor, the isotopic budget can be more tightly constrained observationally, resulting in model simulations which more accurately represent the true atmospheric processes. This also enables water isotope ratios to be leveraged as tools for constraining certain atmospheric processes that are important for the global climate, such as vertical mixing [*Bailey et al*., 2013, 2015b; *Sherwood et al*., 2014]. Beyond this, water isotopes can even be used in a data assimilation framework to constrain and calibrate many different model parameters related to the hydrologic cycle, as was done for parameters in iCLM4 [*Wong*, 2016]. These methods could be extended to the atmosphere as well, and could even be done with both models to better calibrate parameters that influence the coupling between the atmosphere and land surface.

In an attempt to diagnose the root cause of the isotopic precipitation bias in iCAM5, a series of sensitivity experiments were performed to evaluate the degree to which various model processes control the isotopic simulation. It was found that by reducing the frequency with which convection triggers (by increasing the CAPE limit required before deep convection is initiated), the model biases in both vapor and precipitation isotope ratios were improved. However, an interesting result was that for precipitation, the isotopic ratios in the extratropical land and polar regions became significantly higher, even though there was no major change in the local precipitation. Instead, it was found that by decreasing the frequency of deep convection over the midlatitude oceans during winter, higher water isotope ratios were present in the lower troposphere, which in-turn meant that more isotopically enriched water vapor was available to be transported by extratropical cyclones poleward and landward, resulting in an enriched precipitation signal in those

locations. Ultimately, given that these changes improved the isotopic simulation without noticeably degrading the rest of the climate (not shown), it indicates that the current CAPE trigger limit is too low, and that deep convection, at least in certain regions in certain seasons, triggers too frequently. A similar result has been found in previous studies [e.g., *Xie et al*., 2004; *Wang and Zhang*, 2013; *Suhas and Zhang*, 2014], indicating that this result is supported by more than just changes to the water isotope ratios, and that water isotopes can help reveal model parameter choices that improve the model's physical realism. It also has strong implications for examining polar climates using isotope ratios in water, particularly in terms of proxy records of past climates [e.g., *Sime et al*., 2009; *Dee et al*., 2015], as it shows that changes in tropical or midlatitude convective processes, even without a major global temperature change, could produce substantial shifts in the average isotopic ratio of precipitation over the poles and high-latitudes, including Greenland and Antarctica.

Although convection frequency has a strong influence on the water isotopologues, the model is still depleted on average, both in precipitation and in midtropospheric water vapor. The cloud physics is partly responsible, but the overall simulation emerges from the balance between evaporative fluxes at the surface, turbulent exchange, large-scale transport, and precipitation, and the model errors associated with each of these components. While the experiments here have demonstrated significant error in the cloud transport and condensation rates, we have also shown a relationship between the atmospheric transport of water vapor and the simulated convective activity. This implies that large-scale systemic adjustments of the hydrological cycle in CAM5 are essential to improve the isotopic simulation, and consequently improve the underlying hydrology and climate simulations.

Model testing also revealed dynamical biases in the model which could contribute to the errors in the isotopic and hydrologic simulations. For example, it was found that the surface winds were too strong in the subtropics and too weak in the midlatitudes (not shown) when compared to reanalyses. This difference could help explain the bias in ocean surface evaporation, independent of any bias in the atmospheric moisture gradient. It also implies that the lower level winds in the storm track regions may be too weak. Thus, even if the humidity values were correct in the model, the transport of moisture poleward and landward in the midlatitudes would be biased low, producing an isotopic bias similar to the one observed. There could also be biases in atmospheric convergence or divergence, which drive large-scale precipitation production in the atmosphere and thus could produce the biases in precipitation even if the subgrid scale physics behaved perfectly.

Finally, it is unclear what influence the model resolution in the vertical has on water isotopologue values, although vertical transport has been shown to be important for other isotope-enabled models [*Risi et al*., 2012b]. It is also unclear what the impact of using different numerical schemes for resolved-scale advection is, as the analysis presented here used only a finite-volume dynamical core. Ultimately, it has been shown that within the NCAR CESM, the use of water isotopologues, along with more traditional climatological observations, can enable evaluation and development of a more physically realistic and robust model of the water cycle. This work has also provided the community with a new isotopic modeling system to assist in the analysis of water isotopes in the climate system, including paleoclimate proxy records. Combined, these improvements will allow for more accurate and reliable climate projections for both the past and the future.

Acknowledgments

Support for this work came from an NSF graduate fellowship, an NSF Paleoclimate grant AGS-1049104, and a NSF Climate and Large-scale Dynamics grant AGS-0955841 and AGS-1539234. Charles Bardeen was supported by NASA ATTREX grant NNX10AO53A. We gratefully acknowledge support from the NCAR Paleoclimate working group, and particularly Bette Otto-Bliesner, Esther Brady, Mariana Vertenstein, and Andrew Gettelman at NCAR for their ongoing support of this work. We would also like to thank Jiang Zhu for his help with the iCICE4 model, and Sun Wong, who assisted in aspects of the stratiform cloud parameterization. We would also like to thank the two anonymous reviewers whose suggestions improved the clarity and discussion of the results described in this study. Finally, we would like to acknowledge high-performance computing support from Yellowstone (ark:/85065/d7wd3xhc) provided by NCAR's Computational and Information Systems Laboratory, sponsored by the National Science Foundation. The model source code and results used in this study are available from the authors upon request via email to the corresponding author.

References

Bailey, A., D. Toohey, and D. Noone (2013), Characterizing moisture exchange between the Hawaiian convective boundary layer and free troposphere using stable isotopes in water, *J. Geophys. Res. Atmos.*, *118*, 8208–8221, doi:10.1002/jgrd.50639.

Bailey, A., D. Noone, M. Berkelhammer, H. C. Steen-Larsen, and P. Sato (2015a), The stability and calibration of water vapor isotope ratio measurements during long-term deployments, *Atmos. Meas. Tech.*, *8*, 4521–4538, doi:10.5194/amt-8-4521-2015.

Bailey, A., J. Nusbaumer, and D. Noone (2015b), Precipitation efficiency derived from isotope ratios in water vapor distinguishes dynamical and microphysical influences on subtropical atmospheric constituents, *J. Geophys. Res. Atmos.*, *120*, 9119–9137, doi:10.1002/2015JD023403.

Berkelhammer, M., D. C. Noone, T. E. Wong, S. P. Burn, J. F. Knowles, A. Kaushik, P. D. Blanken, and M. W. Williams (2016), Convergent approaches to determine an ecosystem's transpiration fraction, *Global Biogeochem. Cycles*, *30*, 933–951, doi:10.1002/2016GB005392.

Bigeleisen, J. (1961), Statistical mechanics of isotope effects on the thermodynamic properties of condensed systems, *J. Chem. Phys.*, *34*(5), 1485–1493, doi:10.1063/1.1701033.

Bolot, M., B. Legras, and E. J. Moyer (2013), Modelling and interpreting the isotopic composition of water vapour in convective updrafts, *Atmos. Chem. Phys.*, *13*, 7903–7935, doi:10.5194/acp-13-7903-2013.

Bony, S., C. Risi, and F. Vimeux (2008), Influence of convective processes on the isotopic composition (δ^{18}O and δD) of precipitation and water vapor in the tropics: 1. Radiative-convective equilibrium and Tropical Ocean-Global Atmosphere-Coupled Ocean-Atmosphere Response Experiment (TOGA-COARE) simulations, *J. Geophys. Res.*, *113*, D19306, doi:10.1029/2008JD009942.

Browning, K. A. (1971), Radar measurements of air motion near fronts, *Weather*, *26*(8), 320–340, doi:10.1002/j.1477-8696.1971.tb04211.x.

Brutsaert, W. A. (1975a), Theory for local evaporation (or heat transfer) from rough and smooth surfaces at ground level, *Water Resour. Res.*, *11*, 543–550, doi:10.1029/WR011i004p00543.

Brutsaert, W. A. (1975b), The roughness length for water vapor, sensible heat, and other scalars, *J. Atmos. Sci.*, *32*, 2028–2031, doi:10.1175/1520-0469(1975)032 < 2029:TRLFWV>2.0.CO;2.

Cappa, C. D., M. B. Hendricks, D. J. DePaolo, and R. C. Cohen (2003), Isotopic fractionation of water during evaporation, *J. Geophys. Res. Atmos.*, *108*(D16), 4525, doi:10.1029/2003JD003597.

Conroy, J. L., K. M. Cobb, and D. Noone (2013), Comparison of precipitation isotope variability across the tropical Pacific in observations and SWING2 model simulations, *J. Geophys. Res. Atmos.*, *118*, 5867–5892, doi:10.1002/jgrd.50412.

Conroy, J. L., D. Noone, K. M. Cobb, J. W. Moerman, and B. L. Konecky (2016), Paired stable isotopologues in precipitation and vapor: A case study of the amount effect in western tropical Pacific storms, *J. Geophys. Res. Atmos.*, *121*, 3290–3303, doi:10.1002/2015JD023844.

Craig, H., and L. I. Gordon (1965), Deuterium and oxygen 18 variations in the ocean and marine atmosphere, in *Proceedings of the Stable Isotopes in Oceanographic Studies and Paleotemperatures*, edited by E. Tongiogi, pp. 9–130, V. Lishi e F., Pisa, Italy.

Dansgaard, W. (1964), Stable isotopes in Precipitation, *Tellus*, *16*(4), 436–468, doi:10.1111/j.2153-3490.1964.tb00181.x.

Dee, D. P., et al. (2011), The ERA-Interim reanalysis: Configuration and performance of the data assimilation system, *Q. J. R. Meteorol. Soc.*, *137*(656), 553–597, doi:10.1002/qj.828.

Dee, S., J. Emile-Geay, M. N. Evans, A. Allam, E. J. Steig, and D. M. Thompson (2015), PRYSM: An open-source framework for PRoxY System Modeling, with applications to oxygen-isotope systems, *J. Adv. Model. Earth Syst.*, *7*, 1220–1247, doi:10.1002/2015MS000447.

Field, R. D., D. Kim, A. N. LeGrande, J. Worden, M. Kelley, and G. A. Schmidt (2014), Evaluating climate model performance in the tropics with retrievals of water isotopic composition from Aura TES, *Geophys. Res. Lett.*, *41*, 6030–6036, doi:10.1002/2014GL060572.

Frankenberg, C., et al. (2009), Dynamics processes governing lower tropospheric HDO/H_2O ratios as observed from space and ground, *Science*, *325*(5946), 1374–1377, doi:10.1126/science.1173791.

Frankenberg, C., D. Wunch, G. Toon, C. Risi, R. Scheepmaker, J.-E. Lee, P. Wennberg, and J. Worden (2013), Water vapor isotopologue retrievals from high-resolution GOSAT shortwave infrared spectra, *Atmos. Meas. Tech.*, *6*, 263–274, doi:10.5194/amt-6-263-2013.

Gedzelman, S. D., and R. Arnold (1994), Modeling the isotopic composition of precipitation, *J. Geophys. Res. Atmos.*, *99*, 10,455–10,471, doi:10.1029/93JD03518.

Good, S. P., D. Noone, N. Kurita, M. Benetti, and G. J. Brown (2015), D/H isotope ratios in the global hydrologic cycle, *Geophys. Res. Lett.*, *42*, 5042–5050, doi:10.1002/2015GL064117.

Hoffmann, G., M. Werner, and M. Heimann (1998), Water isotope module of the ECHAM atmospheric general circulation model: A study on timescales from days to several years, *J. Geophys. Res. Atmos.*, *103*, 16,871–16,896, doi:10.1029/98JD00423.

Horita, J., and D. J. Wesolowski (1994), Liquid-vapor fractionation of oxygen and hydrogen isotopes of water from the freezing to the critical temperature, *Geochim. Cosmochim. Acta*, *58*(16), 3425–3437, doi:10.1016/0016-7037(94)90096-5.

Hurrell, J. W., J. J. Hack, D. Shea, J. M. Caron, and J. Rosinski (2008), A new sea surface temperature and sea ice boundary dataset for the community atmosphere model, *J. Clim.*, *21*, 5145–5153, doi:10.1175/2008JCLI2292.1.

Hurrell, J. W., et al. (2013), The community earth system model: A framework for collaborative research, *Bull. Am. Meteorol. Soc.*, *94*(9), 1339–1360, doi:10.1175/BAMS-D-12-00121.1.

IAEA/WMO (2016), *Global Network of Isotopes in Precipitation. The GNIP Database*, Vienna, Australia. [Available at http://www.iaea.org/water.]

International Atomic Energy Agency (IAEA) (2012), Monitoring Isotopes in Rivers: Creation of the Global Network of Isotopes in Rivers (GNIR), *IAEA-TECDOC-1673*.

Jones, D. B. A., K. W. Bowman, J. A. Logan, C. L. Heald, J. Liu, M. Luo, J. Worden, and J. Drummond (2009), The zonal structure of tropical O3 and CO as observed by the Tropospheric Emission Spectrometer in November 2004—Part 1: Inverse modeling of CO emissions, *Atmos. Chem. Phys.*, *9*, 547–3562, doi:10.5194/acp-9-3547-2009.

Joussaume, S., R. Sadourny, and J. Jouzel (1984), A general circulation model of water isotope cycles in the atmosphere, *Nature*, *311*, 24–29, doi:10.1038/311024a0.

Jouzel, J., and L. Merlivat (1984), Deuterium and Oxygen 18 in precipitation: Modeling of the isotopic effects during snow formation, *J. Geophys. Res.*, *89*, 11,749–11,757, doi:10.1029/JD089iD07p11749.

Jouzel, J., G. L. Russell, R. J. Suozzo, R. D. Koster, J. W. C. White, and W. S. Broecker (1987), Simulations of the HDO and $H_2^{18}O$ atmospheric cycles using the NASA GISS general circulation model: The seasonal cycle for present-day conditions, *J. Geophys. Res.*, *92*, 14,739–14,760, doi:10.1029/JD092iD12p14739.

Jouzel, J., R. D. Koster, R. J. Suozzo, W. S. Broecker, G. L. Russell, and J. W. C. White (1991), Simulations of the HDO and $H_2^{18}O$ atmospheric cycles using the NASA GISS general circulation model: Sensitivity experiments for present-day conditions, *J. Geophys. Res.*, *96*, 7495–7507, doi:10.1029/90JD02663.

Kurita, N., K. Ichiyanagi, J. Matsumoto, M. D. Yamanaka, and T. Ohata (2009), The relationship between the isotopic content of precipitation and the precipitation amount in tropical regions, *J. Geochem. Explor.*, *102*(3), 113–122, doi:10.1016/j.gexplo.2009.03.002.

Kurita, N., D. Noone, C. Risi, G. A. Schmidt, H. Yamada, and K. Yoneyama (2011), Intraseasonal isotopic variation associated with the Madden-Julian Oscillation, *J. Geophys. Res.*, *116*, D24101, doi:10.1029/2010JD015209.

Lamarque, J.-F., et al. (2010), Historical (1850–2000) gridded anthropogenic and biomass burning emissions of reactive gases and aerosols: Methodology and application, *Atmos. Chem. Phys.*, *10*, 7017–7039, doi:10.5194/acp-10-7017-2010.

Lamarque, J.-F., G. P. Kyle, M. Meinshausen, K. Riahi, S. J. Smith, D. P. van Vuuren, A. J. Conley, and F. Vitt (2011), Global and regional evolution of short-lived raidatively-active gases and aerosols in the Represetative Concentration Pathways, *Clim. Change*, *109*, 191–212, doi:10.1007/s10584-011-0155-0.

Lee, J.-E., I. Fung, D. J. DePaolo, and C. C. Henning (2007), Analysis of the global distribution of water isotopes using the NCAR atmospheric general circulation model, *J. Geophys. Res.*, *112*, D16306, doi:10.1029/2006JD007657.

Lee, J.-E., and I. Fung (2008), "Amount effect" of water isotopes and quantitative analysis of post-condensation processes, *Hydrol. Processes*, *22*(1), 1–8, doi:10.1002/hyp.6637.

LeGrande, A. N., and G. A. Schmidt (2006), Global gridded data set of the oxygen isotopic composition in seawater, *Geophys. Res. Lett.*, *33*, L12604, doi:10.1029/2006GL026011.

Majoube, M. (1971), Fractionnement en oxygène 18 et en deutérium entre l'eau et sa vapeur, *J. Chim. Phys.*, *68*, 1423–1436.

Marshall, J. S., and W. M. Palmer (1948), The distribution of raindrops with size, *J. Meteorol.*, *5*, 165–166, doi:10.1175/1520-0469(1948)005 < 0165:TDORWS>2.0.CO;2.
Meinshausen, M., et al. (2011), The RCP greenhouse gas concentrations and their extensions from 1765 to 2300, *Clim. Change*, *109*, 213–241, doi:10.1007/s10584-011-0156-z.
Merlivat, L. (1978), Molecular diffusivities of $H_2^{16}O$, $HD^{16}O$, and $H_2^{18}O$ in gases, *J. Chem. Phys.*, *69*(6), 2864–2871, doi:10.1063/1.436884.
Merlivat, L., and G. Nief (1967), Isotopic fractionation during change of state solid-vapour and liquid-vapour of water at temperatures below 0°C, *Tellus*, *19*, 122–126.
Merlivat, L., and J. Jouzel (1979), Global climatic interpretation of the deuterium-oxygen 18 relationship for precipitation, *J. Geophys. Res.*, *84*, 5029–5033, doi:10.1029/JC084iC08p05029.
Moerman, J. W., K. M. Cobb, J. F. Adkins, H. Sodemann, B. Clark, and A. A. Tuen (2013), Diurnal to interannual rainfall $\delta^{18}O$ variations in northern Borneo driven by regional hydrology, *Earth Planet. Sci. Lett.*, *369–370*, 108–119, doi:10.1016/j.epsl.2013.03.014.
Moore, M., Z. Kuang, and P. N. Blossey (2014), A moisture budget perspective of the amount effect, *Geophys. Res. Lett.*, *41*(4), 1329–1335, doi:10.1002/2013GL058302.
Morrison, H., and A. Gettelman (2008), A new two-moment bulk stratiform cloud microphysics scheme in the Community Atmosphere Model, Version 3 (CAM3) (2008), Part I: Description and numerical tests, *J. Clim.*, *21*(15), 3542–3659, doi:10.1175/2008JCLI2105.1.
Neale, R. B., et al. (2010), Description of the NCAR Community Atmosphere Model (CAM 5.0), *NCAR Tech. Note Sci. and Tech. Rep, NCAR/TN-486+STR,* NCAR Publ. Off., Boulder, Colo.
Noone, D., and I. Simmonds (2002), Associations between $\delta^{18}O$ of water and climate parameters in a simulation of atmospheric circulation for 1979–95, *J. Clim.*, *15*, 3150–3169, doi:10.1175/1520-0442(2002)015 < 3150:ABOOWA>2.0.CO;2.
Noone, D., and C. Sturm (2010), Comprehensive and dynamical models of global and regional water isotope distributions, in *Isoscapes: Understanding Movement, Patterns and Process on Earth Through Isotope Mapping*, edited by J. West et al., 487 pp., Springer, Netherlands, ISBN: 978-90-481-3353-6.
Park, S., and C. S. Bretherton (2009), The University of Washington shallow convection and moist turbulence schemes and their impact on climate simulations with the community atmosphere model, *J. Clim.*, *22*(12), 3449–3469, doi:10.1175/2008JCLI2557.1.
Park, S., C. S. Bretherton, and P. J. Rasch (2014), Integrating cloud processes in the Community Atmosphere Model, Version 5, *J. Clim.*, *27*, 6821–6856, doi:10.1175/JCLI-D-14-00087.1.
Pruppacher, H. R., and J. D. Klett (1997), *Microphysics of Clouds and Precipitation*, Springer, Norwell, Mass.
Randel, W., E. Moyer, M. Park, E. Jensen, P. Bernath, K. Walker, and C. Boone (2012), Global variations of HDO and HDO/H_2O ratios in the upper troposphere and lower stratosphere derived from ACE-FTS satellite measurements, *J. Geophys. Res.*, *117*, D06303, doi:10.1029/2011JD016632.
Risi, C., S. Bony, and F. Vimeux (2008), Influence of convective processes on the isotopic composition ($\delta^{18}O$ and δD) of precipitation and water vapor in the tropics. 2: Physical interpretation of the amount effect, *J. Geophys. Res.*, *113*, D19306, doi:10.1029/2008JD009943.
Risi, C., et al. (2012a), Process-evaluation of tropospheric humidity simulated by general circulation models using water vapor isotopologues. 1: Comparison between models and observations, *J. Geophys. Res.*, *117*, D05303, doi:10.1029/2011JD016621.
Risi, C., et al. (2012b), Process-evaluation of tropospheric humidity simulated by general circulation models using water vapor isotopic observations. 2: Using isotopic diagnostics to understand the mid and upper tropospheric moist bias in the tropics and subtropics, *J. Geophys. Res.*, *117*, D05304, doi:10.1029/2011JD016623.
Rodger, R. R., and M. K. Yau (1989), *A Short Course in Cloud Physics*, 3rd ed., Elsevier, Burlington, Mass.
Scheepmaker, R. A., C. Frankenberg, A. Galli, A. Butz, H. Schrijver, N. M. Deutscher, D. Wunch, T. Warneke, S. Fally, and I. Aben (2013), Improved water vapour spectroscopy in the 4174–4300 cm^{-1} region and its impact on SCIAMACHY HDO/H_2O measurements, *Atmos. Meas. Tech.*, *6*, 879–894, doi:10.5194/amt-6-879-2013.
Scheepmaker, R. A., et al. (2015), Validation of SCIAMACHY HDO/H_2O measurements using the TCCON and NDACC-MUSICA networks, *Atmos. Meas. Tech.*, *8*, 1799–1818, doi:10.5194/amt-8-1799-2015.
Sherwood, S., R. Roca, T. M. Weckwerth, and N. G. Andronova (2010), Tropospheric water vapor, convection, and climate, *Rev. Geophys.*, *48*, RG2001, doi:10.1029/2009RG000301.
Sherwood, S. C., S. Bony, and J.-L. Dufresne (2014), Spread in model climate sensitivity traced to atmospheric convective mixing, *Nature*, *505*, 37–42, doi:10.1038/nature12829.
Sime, L. C., E. W. Wolff, K. I. C. Oliver, and J. C. Tindall (2009), Evidence for warmer interglacials in East Antarctic ice cores, *Nature*, *462*, 342–345, doi:10.1038/nature08564.
Stewart, M. K. (1975), Stable isotope fractionation due to evaporation and isotopic exchange of falling waterdrops: Applications to atmospheric processes and evaporation of lakes, *J. Geophys. Res.*, *80*, 1133–1146, doi:10.1029/JC080i009p01133.
Straka, J. M. (2009), *Cloud and Precipitation Microphysics: Principles and Parameterizations*, Cambridge Univ. Press, Cambridge, U. K.
Suhas, E., and G. J. Zhang (2014), Evaluation of trigger functions for convective parameterization schemes using observations, *J. Clim.*, *27*, 7647–7666, doi:10.1175/JCLI-D-13-00718.1.
Wang, X., and M. Zhang (2013), An analysis of parameterization interactions and sensitivity of single-column model simulations to convection schemes in CAM4 and CAM5, *J. Geophys. Res. Atmos.*, *118*, 8869–8880, doi:10.1002/jgrd.50690.
Williams, C. R., and K. S. Gage (2009), Raindrop size distribution variability estimated using ensemble statistics, *Ann. Geophys.*, *27*, 555–567, doi:10.5194/angeo-27-555-2009.
Winkler, R., A. Landais, C. Risi, M. Baroni, A. Ekaykin, J. Jouzel, J. P. Petit, F. Prie, B. Minster, and S. Falourd (2013), Interannual variation of water isotopologues at Vostok indicates a contribution from stratospheric water vapor, *Proc. Natl. Acad. Sci. U. S. A.*, *110*(44), 17,674–17,679, doi:10.1073/pnas.1215209110.
Wong, T. (2016), The impact of stable water isotopic information on parameter calibration in a land surface model, Doctoral dissertation, Univ. of Colorado, Boulder, Colo., doi:10.13140/RG.2.2.30181.40162.
Wong, T., J. Nusbaumer, and D. Noone (2017), Evaluation of modeled land-atmosphere exchanges with a comprehensive water isotope fractionation scheme in version 4 of the Community Land Model, *J. Adv. Model. Earth Syst*., doi:10.1002/2016MS000842.
Worden, J., et al. (2006), Tropospheric Emission Spectrometer observations of the tropospheric HDO/H_2O ratio: Estimation approach and characterization, *J. Geophys. Res.*, *111*, D16309, doi:10.1029/2005JD006606.
Worden, J., D. Noone, J. Galewsky, A. Bailey, K. Bowman, D. Brown, J. Hurley, S. Kulawik, J. Lee, and. M. Strong (2011), Estimate of bias in Aura TES HDO/H_2O profiles from comparison of TES and in situ HDO/H_2O measurements at the Mauna Loa observatory, *Atmos. Chem. Phys.*, *11*, 4491–4503, doi:10.5194/acp-11-4491-2011.

Xie, S., M. Zhang, J. S. Boyle, R. T. Cederwall, G. L. Potter, and W. Lin (2004), Impact of a revised convective triggering mechanism on Community Atmosphere Model, Version 2, simulations: Results from short-range weather forecasts, *J. Geophys. Res.*, *109*, D14102, doi:10.1029/2004JD004692.

Yoshimura, K., M. Kanamitsu, D. Noone, and T. Oki (2008), Historical isotope simulation using Reanalysis atmospheric data, *J. Geophys. Res.*, *113*, D19108, doi:10.1029/2008JD010074.

Yoshimura, K., C. Frankenberg, J. Lee, M. Kanamitsu, J. Worden, and T. Röckmann (2011), Comparison of an isotopic atmospheric general circulation model with new quasi-global satellite measurements of water vapor isotopologues, *J. Geophys. Res.*, *116*, D19118, doi:10.1029/2011JD016035.

Zhang, G. J., and N. A. McFarlane (1995), Sensitivity of climate simulations to the parameterization of cumulus convection in the Canadian climate centre general circulation model, *Atmos. Ocean*, *33*(3), 407–446, doi:10.1080/07055900.1995.9649539.

Erratum

Due to a transcription error, Equation (14) was incorrectly presented in the originally published version of this file. The correct equation was used in the model, and the error had no impact on the results or analysis published. All corrections have been made to the online version, but not the PDF, and the online version may be considered the autoritative version of record.

$$q_i = (q_{i0} + L_{i0}) * \frac{1}{\alpha_e\left(\frac{1}{\Gamma} - 1\right) + 1}, \quad \Gamma = \frac{q}{q + L} \tag{14}$$